**5512** *Inorg. Chem.* **2009**, *48*, 5512–5525
DOI: 10.1021/ic900654m

Inorganic Chemistry
Article

# Self-Assembly of the First Discrete 3d−4f−4f Triple-Stranded Helicate

**Thomas Riis-Johannessen,*[,†,∥] Gérald Bernardinelli,[‡] Yaroslav Filinchuk,[§] Sarah Clifford,[†] Natalia Dalla Favera,[†] and Claude Piguet*[,†]**

[†]*Department of Inorganic, Analytical and Applied Chemistry, University of Geneva, 30 quai E. Ansermet, CH-1211 Geneva 4, Switzerland,* [‡]*Laboratory of X-ray Crystallography, University of Geneva, 24 quai E. Ansermet, CH-1211 Geneva 4, Switzerland, and* [§]*Swiss-Norwegian Beamlines (SNBL) at the European Synchrotron Radiation Facility (ESRF), 6 rue Jules Horowitz, F-38043 Grenoble, France.* [∥] *Current address: Swiss Federal Institute of Technology Lausanne (EPFL), CH-1015 Lausanne, Switzerland.*

Received April 3, 2009

The connection of an additional bidentate chelating unit at the extremity of a segmental bis-tridentate ligand in **L5** provides an unprecedented sequence of binding sites for the self-assembly of heterometallic 3d−4f triple-stranded helicates. Thorough thermodynamic and structural investigations in acetonitrile show the formation of intricate mixtures of complexes when a single type of metal (3d or 4f) is reacted with **L5**. However, the situation is greatly simplified when Zn(II) (3d-block) and Lu(III) (4f-block) are simultaneously coordinated to **L5**, thus leading to only two identified species: the target $C_3$-symmetrical trinuclear triple-stranded d−f−f helicate *HHH*-$[ZnLu_2(\mathbf{L5})_3]^{8+}$ and a tetranuclear double-stranded complex $[Zn_2Lu_2(\mathbf{L5})_2]^{10+}$. Interestingly, the removal of Zn(II) from the former triple-helical complex has only a minor effect on the coordination of Lu(III), and translational autodiffusion coefficients show a simple reduction of the length of the molecular rigid cylinder from $L = 2.7$ nm in *HHH*-$[ZnLu_2(\mathbf{L5})_3]^{8+}$ to $L = 2.3$ nm in *HHH*-$[Lu_2(\mathbf{L5})_3]^{6+}$. Finally, the complete thermodynamic picture provides five novel stability macroconstants containing information about short-range (ca. 9 Å) and long-range (ca. 18 Å) intramolecular intermetallic d−f and f−f interactions.

## Introduction

Is it justified to prepare one more polynuclear triple-stranded helicate? This question is fully licit when we consider that (i) the first empirical reports of binuclear triple-stranded helicates with Cu(II)[1] or Fe(III)[2] were made more than three decades ago and (ii) the first planned synthesis of a binuclear Co(II) triple-stranded helicate followed in 1991.[3] Since then, a plethora of homometallic triple-stranded helicates with d-block or f-block metals have been described.[4] However, it is fair to note that, except for the pioneering work of Piguet and co-workers,[5,6] only limited efforts have been focused on the simultaneous introduction of 3d- and 4f-block cations into triple-helical complexes.[7,8] Moreover, all isolated and structurally characterized d−f helicates correspond to binuclear $[MLn(\mathbf{L}k)_3]$ systems, in which $\mathbf{L}k$ ($k = 1-3$, Chart 1) is a segmental ligand with its bidentate site coordinated to the pseudo-octahedral d-block cation (M = Ti(IV), Cr(III), Fe(II), Co(II), Co(III), Zn(II)) and its tridentate site bound to the pseudo-tricapped trigonal prismatic lanthanide (Ln = La−Lu, except Pm).[5−7]

To the best of our knowledge, the introduction of two 4f- and one 3d-block metals into a trinuclear triple-stranded helicate has been achieved only once in the complex $[GdFeGd(\mathbf{L4}\text{-}4H)_3]^{3-}$,

*To whom correspondence should be addressed. E-mail: thomas.riis-johannessen@epfl.ch (T.R.-J.), Claude.Piguet@unige.ch (C.P.).

(1) Harris, C. M.; McKenzie, E. D. *J. Chem. Soc. A* **1969**, 746–753.
(2) (a) Carrano, C. J.; Raymond, K. N. *J. Am. Chem. Soc.* **1978**, *100*, 5371–5374. (b) Carrano, C. J.; Cooper, S. J.; Raymond, K. N. *J. Am. Chem. Soc.* **1979**, *101*, 599–604. (c) Scarrow, R. C.; White, D. L.; Raymond, K. N. *J. Am. Chem. Soc.* **1985**, *107*, 6540–6546.
(3) Williams, A. F.; Piguet, C.; Bernardinelli, G. *Angew. Chem., Int. Ed. Engl.* **1991**, *30*, 1490–1492.
(4) For comprehensive reviews, see: (a) Piguet, C.; Bernardinelli, G.; Hopfgartner, G. *Chem. Rev.* **1997**, *97*, 2005–2062. (b) Albrecht, M. *Chem. Rev.* **2001**, *101*, 3457–3497. (c) Hannon, M. J.; Childs, L. J. *Supramol. Chem.* **2004**, *16*, 7–22. (d) Albrecht, M.; Fröhlich, R. *Bull. Chem. Soc. Jpn.* **2007**, *80*, 797–808.
(5) (a) Piguet, C.; Rivara-Minten, E.; Hopfgartner, G.; Bunzli, J.-C. G. *Helv. Chim. Acta* **1995**, *78*, 1541–1566. (b) Piguet, C.; Rivara-Minten, E.; Hopfgartner, G.; Bunzli, J.-C. G. *Helv. Chim. Acta* **1995**, *78*, 1651–1672.
(6) (a) Piguet, C.; Bunzli, J.-C. G.; Bernardinelli, G.; Hopfgartner, G.; Petoud, S.; Schaad, O. *J. Am. Chem. Soc.* **1996**, *118*, 6681–6697. (b) Piguet, C.; Rivara-Minten, E.; Bernardinelli, G.; Bunzli, J.-C. G.; Hopfgartner, G. *J. Chem. Soc., Dalton Trans.* **1997**, 421–433. (c) Rigault, S.; Piguet, C.; Bernardinelli, G.; Hopfgartner, G. *Angew. Chem., Int. Ed. Engl.* **1998**, *37*, 169–172. (d) Cantuel, M.; Bernardinelli, G.; Imbert, D.; Bunzli, J.-C. G.; Hopfgartner, G.; Piguet, C. *J. Chem. Soc., Dalton Trans.* **2002**, 1929–1940. (e) Cantuel, M.; Gumy, F.; Bunzli, J.-C. G.; Piguet, C. *Dalton Trans.* **2006**, 2647–2660.
(7) Albrecht, M.; Liu, Y.; Zhu, S. S.; Schalley, C. A.; Fröhlich, R. *Chem. Commun.* **2009**, 1195–1197.
(8) Pierre, V. C.; Botta, M.; Aime, S.; Raymond, K. N. *J. Am. Chem. Soc.* **2006**, *128*, 9272–9273.

 Published on Web 05/14/2009 

**Chart 1.** Chemical Structures of Ligands **L1**−**L4** (B = Bidentate Binding Site, T = Tridentate Binding Site)

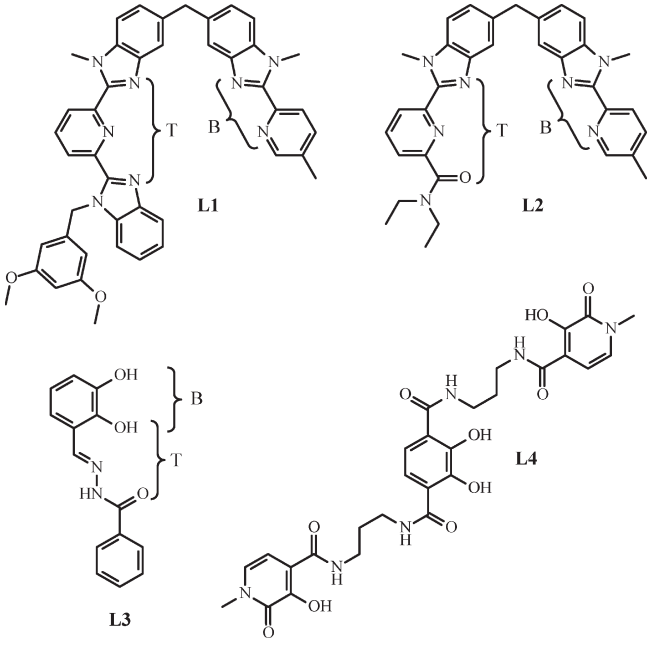


whose existence in water was postulated on the basis of gas-phase electrospray ionization mass spectrometry (ESI-MS) spectra and solution nuclear magnetic relaxation dispersion profiles (Chart 1).[8] Beyond the novel directional electronic and photophysical properties expected for the replacement of the $C_2$-symmetrical f−d−f arrangements of the metals in the latter complex with an unprecedented d−f−f sequence in the target triple-stranded helicate *HHH*-$[MLn_2(\mathbf{L5})_3]^{8+}$ (Figure 1a, *HHH* stands for head-to-head-to-head),[9] the current challenge of unraveling the thermodynamic and structural parameters controlling cooperativity[10] and preorganization[11] in (supra)-molecular multicomponent assemblies requires additional experimental data, in which a maximum number of different intramolecular intermetallic interactions operates (Figure 1b).[12]

The formation of the planned complex *HHH*-$[MLn_2(\mathbf{L5})_3]^{8+}$ indeed provides pertinent information on two different geminal intermetallic interactions operating at ca. 9 Å ($\Delta E_{1-2}^{M,Ln}$ and $\Delta E_{1-2}^{Ln,Ln}$) and one vicinal interaction effective at ca. 18 Å ($\Delta E_{1-3}^{M,Ln}$, Figure 1). However, a satisfying description of the thermodynamic formation constant of *HHH*-$[MLn_2(\mathbf{L5})_3]^{8+}$ ($\beta_{1,2,3}^{M,Ln,L5}$ in eq 1) requires a minimum set of eight microscopic parameters: the three different intermetallic interactions mentioned above and also three different

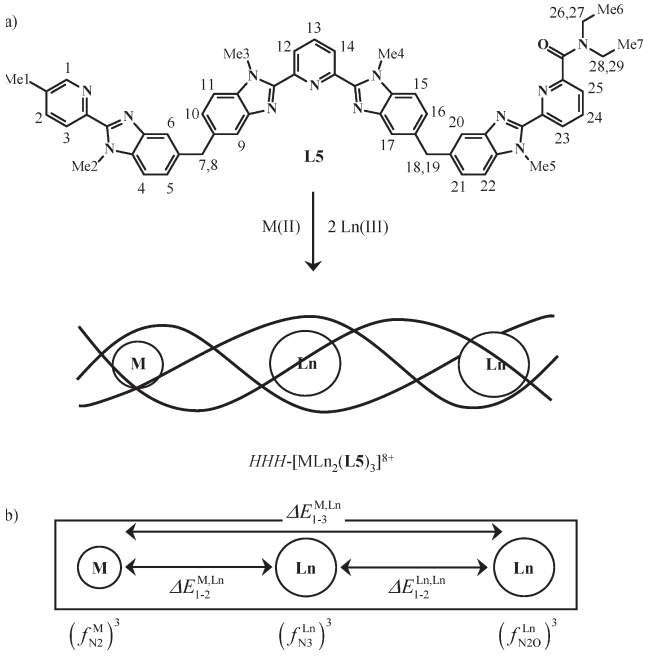


**Figure 1.** (a) Planned self-assembly of the bimetallic trinuclear d−f−f triple-stranded helicate *HHH*-$[MLn_2(\mathbf{L5})_3]^{8+}$ (numbering scheme for $^1$H NMR data) and (b) selected microscopic descriptors required for the thermodynamic modeling of the formation constant of *HHH*-$[MLn_2(\mathbf{L5})_3]^{8+}$ ($f_i^R$ is the affinity of site *i* for the metal R (R = M, Ln), $\Delta E_{1-\alpha}^{R1,R2}$ are the intramolecular R1···R2 intermetallic interactions operating at short (geminal ≈ 9 Å, α = 2) or long distances (vicinal ≈ 18 Å, α = 3; R1, R2 = M, Ln).

metal−ligand affinities ($f_{N2}^M$, $f_{N3}^{Ln}$, and $f_{N2O}^{Ln}$, Figure 1b), one effective concentration measuring the intramolecular macrocyclization of two adjacent binding units, and one interligand interaction measuring the extra free energy change which results when two or more binding units are connected to the same metal.[12]

$$3\mathbf{L5} + M^{2+} + 2Ln^{3+} \rightleftharpoons [MLn_2(\mathbf{L5})_3]^{8+} \quad \log \beta_{1,2,3}^{M,Ln,L5} \tag{1}$$

In view of this, the determination of $\log \beta_{1,2,3}^{M,Ln,L5}$ is not sufficient to unravel the different contributions to the assembly process. The simultaneous consideration of thermodynamic constants collected for a large number of closely related systems possessing identical topologies and structures (i.e., (i) with identical diphenylmethane spacers fixing the intermetallic separation to 9 Å and (ii) with the unique set of the three binding units $N_2$, $N_3$, and $N_2O$ found in **L1** and **L2**, Chart 1), therefore, represents an elegant approach for addressing this challenge.[12] During the past decade, we have systematically collected thermodynamic data on Zn(II) and Lu(III) triple-stranded helicates with ligands **L1** and **L2** (Chart 1)[5,6] and **L6**−**L12** (Chart 2),[13−15] but the total number of identified stability constants is currently insufficient

(9) Torelli, S.; Imbert, D.; Cantuel, M.; Bernardinelli, G.; Delahaye, S.; Hauser, A.; Bunzli, J.-C. G.; Piguet, C. *Chem.Eur. J.* **2005**, *11*, 3228–3242.

(10) (a) Ercolani, G. *J. Am. Chem. Soc.* **2003**, *125*, 16097–16103. (b) Hamacek, J.; Borkovec, M.; Piguet, C. *Dalton Trans.* **2006**, 1473–1490. (c) Steed, J. W.; Atwood, J. L. *Supramolecular Chemistry*, 2nd ed.; John Wiley & Sons, Ltd: New York, **2009**; Chapter 10.

(11) (a) Ercolani, G. *J. Phys. Chem. B* **2003**, *107*, 5052–5057. (b) Mulder, A.; Huskens, J.; Reinhoudt, D. N. *Org. Biomol. Chem.* **2004**, *2*, 3409–3424. (c) Badjic, J. D.; Nelson, A.; Cantrill, S. J.; Turnbull, W. B.; Stoddart, J. F. *Acc. Chem. Res.* **2005**, *38*, 723–732. (d) Ercolani, G. *Struct. Bonding (Berlin)* **2006**, *121*, 167–215. (e) Fyles, T. M.; Tong, C. C. *New J. Chem.* **2007**, *31*, 296–304. (f) Chekmeneva, E.; Hunter, C. A.; Packer, M. J.; Turega, S. M. *J. Am. Chem. Soc.* **2008**, *130*, 17718–17725.

(12) Dalla Favera, N.; Hamacek, J.; Borkovec, M.; Jeannerat, D.; Gumy, F.; Bunzli, J.-C. G.; Ercolani, G.; Piguet, C. *Chem.Eur. J.* **2008**, *14*, 2994–3005.

(13) Piguet, C.; Bernardinelli, G.; Bocquet, B.; Quattropanni, A.; Williams, A. F. *J. Am. Chem. Soc.* **1992**, *114*, 7440–7451.

(14) (a) Piguet, C.; Bunzli, J.-C. G.; Bernardinelli, G.; Hopfgartner, G.; Williams, A. F. *J. Am. Chem. Soc.* **1993**, *115*, 8197–8206. (b) Zeckert, K.; Hamacek, J.; Rivera, J.-P.; Floquet, S.; Pinto, A.; Borkovec, M.; Piguet, C. *J. Am. Chem. Soc.* **2004**, *126*, 11589–11601.

(15) Floquet, S.; Ouali, N.; Bocquet, B.; Bernardinelli, G.; Imbert, D.; Bunzli, J.-C. G.; Hopfgartner, G.; Piguet, C. *Chem.Eur. J.* **2003**, *9*, 1860–1875.

**Chart 2.** Chemical Structures of Ligands **L6**−**L12**

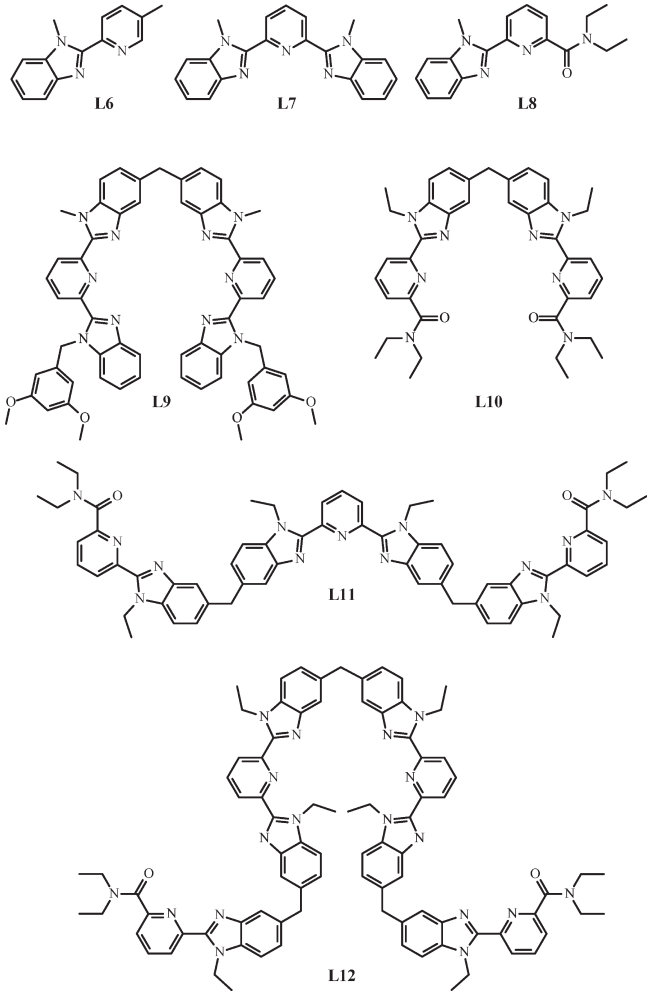


for fitting the various intermetallic interactions without imposing arbitrary Coulombic constraints defined by the intermetallic distances.[12] Indeed, the latter assumption is now known to be inadequate because of the significant contribution of solvation processes to this type of microscopic parameter.[16] It is therefore crucial to obtain additional thermodynamic data for the complexes of **L5**, a ligand which contains (i) two diphenylmethane spacers, (ii) three different binding sites, and (iii) the capacity of loading different metal ions with variable point charges along the helical axis. As an ultimate step prior to the global and unconstrained determination of the microscopic parameters controlling the assembly processes of ligands **L1**, **L2**, and **L5**−**L12** with Zn(II) and Lu(II), we report here on the detailed structural and thermodynamic investigation of the missing complexes obtained between **L5** and the latter two cations in acetonitrile.

## Results and Discussion

**Synthesis and Structural Characterization of Ligand L5 and of its Complex *HHH*-[ZnLu$_2$(L5)$_3$](CF$_3$SO$_3$)$_8$.** The tritopic ligand **L5** is prepared in three steps from the previously reported compounds **L2** and **1** (Scheme 1).[6a] Quantitative hydrolysis of **L2** is first achieved under strongly basic conditions to give the monocarboxylic acid **2**.[17] Acylation of **2** followed by coupling with the substituted *o*-nitroamine **1** then occurs in moderate yield (60−70%) to give the precursor **3**, which, upon reductive cyclization with iron, affords **L5** in respectable yield (80%).

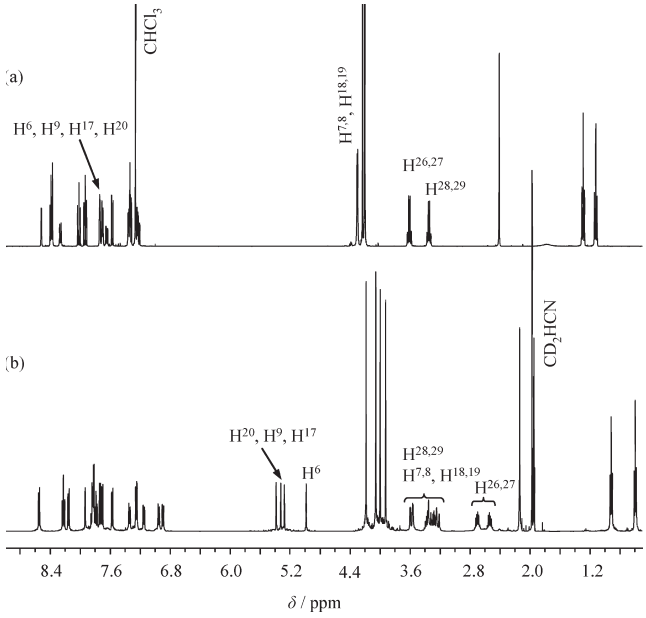


**Figure 2.** $^1$H NMR spectra of (a) **L5** in $CDCl_3$ and (b) *HHH*-[ZnLu$_2$(**L5**)$_3$]$^{8+}$ in $CD_3CN$ (298 K). See Figure 1a for proton numbering.

**Scheme 1.** Synthesis of Ligand **L5**

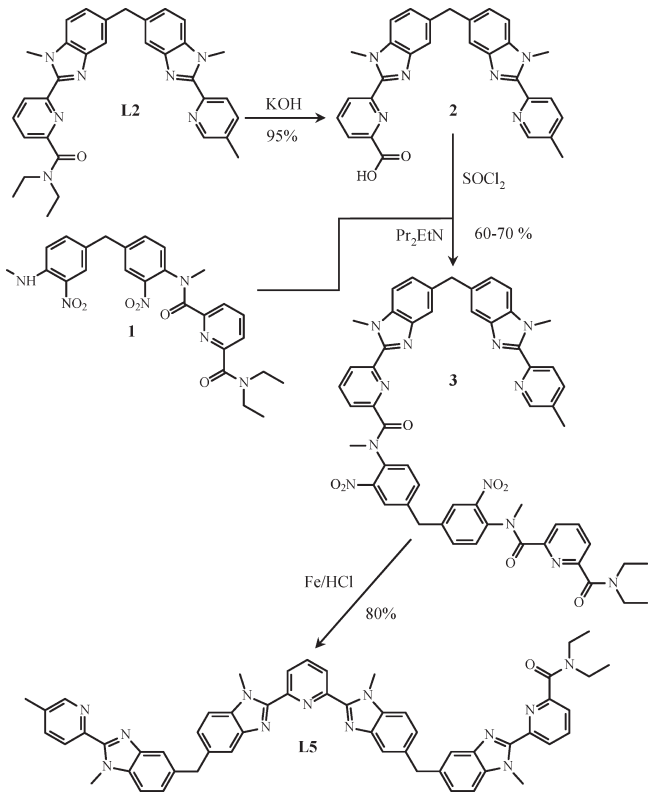


(16) Canard, G.; Piguet, C. *Inorg. Chem.* **2007**, *46*, 3511–3522.

(17) Edder, C.; Piguet, C.; Bunzli, J.-C. G.; Hopfgartner, G. *J. Chem. Soc., Dalton Trans.* **1997**, 4657–4663.

**Table 1.** $^1$H NMR Chemical Shifts for **L5** ($CDCl_3$) and Complexes *HHH*-$[ZnLu_2(\mathbf{L5})_3]^{8+}$ and *HHH*-$[Lu_2(\mathbf{L5})_3]^{6+}$ (2:1 $CD_3CN/CDCl_3$)[a]

| | bidentate binding site | | | | | | | | |
|---|---|---|---|---|---|---|---|---|---|
| | $H^1$ | $H^2$ | $H^3$ | $H^4$ | $H^5$ | $H^6$ | $Me^1$ | $Me^2$ | $H^{7,8}$ |
| **L5** | 8.51 | 7.64 | 8.25 | 7.32 | 7.21 | 7.69 | 2.41 | 4.23 | 4.29 |
| *HHH*-$[ZnLu_2(\mathbf{L5})_3]^{8+}$ | 7.93 | 7.83 | 8.15 | 7.26 | 6.89 | 7.34 | 2.14 | 4.06 | 3.58/3.23 |
| *HHH*-$[Lu_2(\mathbf{L5})_3]^{6+}$ | 8.55 | 7.62 | 8.10 | 7.10 | 6.73 | 6.90 | 2.35 | 4.03 | 3.60/3.41 |

| | tridentate binding site ($N_3$) | | | | | | | | | | | |
|---|---|---|---|---|---|---|---|---|---|---|---|---|
| | $H^9$ | $H^{10}$ | $H^{11}$ | $H^{12}$ | $H^{13}$ | $H^{14}$ | $H^{15}$ | $H^{16}$ | $H^{17}$ | $H^{18,19}$ | $Me^3$ | $Me^4$ |
| **L5** | 7.73 | 7.25 | 7.35 | 8.38 | 8.01 | 8.38 | 7.34 | 7.24 | 7.72 | 4.31 | 4.21 | 4.19 |
| *HHH*-$[ZnLu_2(\mathbf{L5})_3]^{8+}$ | 5.33 | 7.15 | 7.57 | 7.83 | 7.82 | 7.78 | 7.70 | 7.34 | 5.27 | 3.58/3.34 | 4.00 | 3.92 |
| *HHH*-$[Lu_2(\mathbf{L5})_3]^{6+}$ | 5.79 | 7.06 | 7.17 | 7.33 | 7.72 | 7.62 | 7.64 | 7.28 | 5.12 | 3.50/3.27 | 3.69 | 3.86 |

| | tridentate binding site ($N_2O$) | | | | | | | | | | |
|---|---|---|---|---|---|---|---|---|---|---|---|
| | $H^{20}$ | $H^{21}$ | $H^{22}$ | $H^{23}$ | $H^{24}$ | $H^{25}$ | $H^{26,27}$ | $H^{28,29}$ | $Me^5$ | $Me^6$ | $Me^7$ |
| **L5** | 7.70 | 7.24 | 7.33 | 8.39 | 7.93 | 7.57 | 3.61 | 3.35 | 4.19 | 1.29 | 1.12 |
| *HHH*-$[ZnLu_2(\mathbf{L5})_3]^{8+}$ | 5.39 | 6.95 | 7.26 | 8.55 | 8.22 | 7.74 | 2.70/2.55 | 3.37/3.28 | 4.19 | 0.60 | 0.92 |
| *HHH*-$[Lu_2(\mathbf{L5})_3]^{6+}$ | 5.29 | 6.91 | 7.22 | 8.51 | 8.20 | 7.68 | 2.67/2.52 | 3.33/3.25 | 4.16 | 0.60 | 0.91 |

[a] See Figure 1a for proton numbering.

The $^1$H NMR spectrum of the free ligand in $CDCl_3$ (Figure 2a) shows a total of 21 signals for the aromatic protons ($\delta$ 7.1−8.6 ppm), some of which are superimposed, a further four signals for the methylene protons ($\delta$ 3.3−4.4 ppm), and seven signals for the methyl groups ($\delta$ 1.1−4.3 ppm), consistent with it adopting a time-averaged $C_s$ symmetry in an ambient temperature solution. All signals have been assigned with the use of 2D correlation spectra showing scalar spin−spin ({$^1$H−$^1$H} COSY; COSY = correlation spectroscopy) and dipole−dipole ({$^1$H−$^1$H} NOESY and ROESY; NOESY = nuclear Overhauser enhancement spectroscopy, ROESY = rotating-frame Overhauser enhancement spectroscopy) couplings (Table 1). The absence of through-space NOE effects between pairs of protons $H^3/Me^2$, $H^{12}/Me^3$, $H^{14}/Me^4$, and $H^{23}/Me^5$ (numbering in Figure 1a) suggests that adjacent *N*-heterocyclic rings along the strand adopt the standard trans−trans conformation in solution, as observed for related oligo-heterocyclic ligands.[5,6,14,15]

The reaction of **L5** (3 equiv, $|\mathbf{L5}|_{tot} = 10^{-3}$ M) with stoichiometric amounts of diamagnetic $Zn(CF_3SO_3)_2$ (1 equiv) and $Lu(CF_3SO_3)_3$ (2 equiv) in acetonitrile gives a pale yellow solution for which ESI-MS shows peaks at *m*/*z* 566.6 (15%), 709.5 (90%), 924.0 (100%), 1282.1 (20%), and 1997.1 (5%), corresponding to molecular ions of the general formula $[ZnLu_2(\mathbf{L5})_3(CF_3SO_3)_x]^{(8-x)+}$ (*x* takes integer values in the range $2 \leq x \leq 6$).

The $^1$H NMR spectrum recorded in $CD_3CN$ (Figure 2b) is consistent with the quantitative formation of a $C_3$-symmetric triple-stranded helicate structure in solution, whereby three strands of **L5** coordinate the three metals in a head-to-head-to-head (*HHH*-) fashion. All methylene protons ($H^{7,8}$, $H^{18,19}$, $H^{26,27}$, and $H^{28,29}$, Figure 2b) are rendered diastereotopic due to the permanent loss of mirror symmetry on going from the free to the complexed ligand conformations. Pronounced NOE effects between proton pairs $H^3/Me^2$, $H^{12}/Me^3$, $H^{14}/Me^4$, and $H^{23}/Me^5$ evidence the usual interannular trans−trans to cis−cis conformational changes required for three adjacent *N*-heterocycles to coordinate to a common metal ion.[5,6] The observed additional NOE effects, involving protons $H^5/Me^3$, $H^6/Me^2$, $H^{7,8}/Me^2$, $H^{18,19}/Me^5$, and $H^{21}/Me^4$, can be assigned to interligand through-space interactions, a consequence of the ligand strands being tightly wrapped about the helical axis.[5,6] A final diagnostic for the expected helicate structure in $[ZnLu_2(\mathbf{L5})_3]^{8+}$ is the unusually low frequencies ($4.8 \leq \delta \leq 5.5$ ppm) at which aromatic protons $H^6$, $H^9$, $H^{17}$, and $H^{20}$ resonate because of their location within the shielding region of the benzimidazole rings on an adjacent ligand strand in the final helicate assembly.[5,6] Slow diffusion of *n*-hexane vapor into a 10 mM solution of **L5** (3 equiv), $Zn(CF_3SO_3)_2$ (1 equiv), and $Lu(CF_3SO_3)_3$ (2 equiv) in methanol gave pale yellow prisms for which elemental analyses, after isolation, were consistent with the formulation $[ZnLu_2(\mathbf{L5})_3](CF_3SO_3)_8 \cdot xH_2O$ ($10 \leq x \leq 14$, depending on the batch). The crystals were extremely fragile and susceptible to solvent loss on removal from the mother liquor. Those selected for X-ray diffraction studies diffracted poorly, and sufficient intensity for a structural analysis was only obtained using synchrotron radiation. Even then, however, the best data set from a variety of different attempts was of limited quality, and consequently the model does not merit detailed analysis beyond establishing the basic atomic connectivity and shape of the complex cation (Figure 3). The crystal structure was solved in $P\bar{1}$ and comprises columns of canted *HHH*-$[ZnLu_2(\mathbf{L5})_3]^{8+}$ cations which propagate along the crystallographic [001] direction. These columns are not closely packed: large channels of ca. 12 Å in diameter are left to accommodate highly disordered counterions and solvent molecules. The apparent porosity offers a likely explanation for the extremely rapid degradation of the crystals on removal from the mother liquor: the channels essentially provide a means for the co-crystallized solvent to escape, a process which results in the partial collapse of the crystal lattice. The cationic part of the asymmetric unit consists of three strands of **L5** wrapped about a helical axis defined by the Zn(II) and two Lu(III) ions to give the expected bimetallic trinuclear helicate *HHH*-$[ZnLu_2(\mathbf{L5})_3]^{8+}$. The Zn(II) and Lu(III) ions occupy, respectively, distorted octahedral

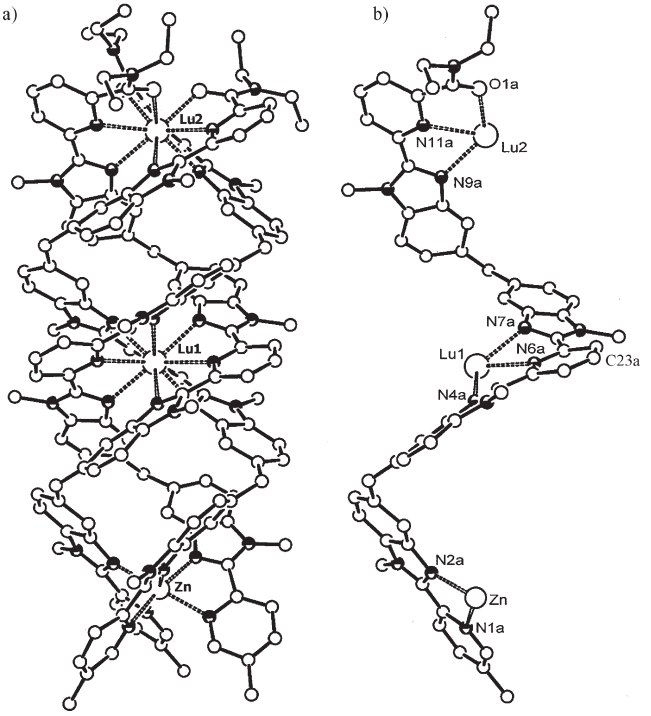


**Figure 3.** (a) Solid-state molecular structure of the complex cation *HHH*-$[ZnLu_2(\mathbf{L5})_3]^{8+}$ showing (b) partial atom numbering scheme for ligand strand A.

and pseudo-tricapped trigonal prismatic (ttp) sites provided by (i) three $N_2$ chelates for Zn(II), (ii) three $N_3$ chelates for Lu1, and (iii) three $N_2O$ chelates for Lu2, as presented by the three co-aligned strands of **L5**. Selected metric parameters for the structure are listed in Tables S1−S4 in the Supporting Information, though caution must be exercised in analyzing these data, the most noteworthy (and reliable) of which are those concerning the strongly scattering metal atoms. Nonbonded distances for the latter are Zn−Lu1 = 8.78(1) Å and Lu1−Lu2 = 8.93(1) Å, with a Zn−Lu1−Lu2 angle of 178.1 (5)°, characteristic of a linear helical axis. We note that these values are typical of the geminal (1−2) separations between cations in neighboring sites of polynuclear helicates based on segmental *oligo*-pyridyl-benzimidazole ligands, as illustrated by the now abundant collection of bi-, tri-, and tetranuclear helicates based on ligands **L2**, **L9**−**L12**, for which analogous distances lie in the range 8.86−9.41 Å.[6,12−15]

Taking now the molecular structure of *HHH*-$[ZnLu_2(\mathbf{L5})_3]^{8+}$ obtained in the solid state as a model for the $C_3$-symmetrical complex in solution, we can build the Connolly surface accessible to solvent molecules (probe radius = 2.0 Å for acetonitrile, $V_{CH_3CN}$ = 34 Å$^3$),[18] from which the associated Connolly volume limited by this surface can be estimated: $V_{ZnLu2}^{Connolly}$ = 2839 Å$^3$. The use of eq 2 then yields the spherical equivalent radius of *HHH*-$[ZnLu_2(\mathbf{L5})_3]^{8+}$ ($r_{eq}^{ZnLu2}$ = 8.8 Å),[19] which can be compared with the experimental hydrodynamic radius $r_H^{ZnLu2}$ via the shape factor $f(p)$ (eq 3).[20]

$$r_{eq}^{x} = \sqrt[3]{\frac{3V_x^{Connolly}}{4\pi}} \quad (2)$$

$$r_H^x = r_{eq}^x / f(p) \quad (3)$$

The hydrodynamic radius is itself usually deduced from the determination of the translational autodiffusion coefficient $D_x$ by using the Stokes−Einstein equation, eq 4, wherein $k$ is Boltzmann's constant, $T$ is the temperature, and $\eta$ is the viscosity of the solvent ($\eta$ = 3.65 × 10$^{-4}$ kg m$^{-1}$ s$^{-1}$ for acetonitrile at 293 K).[21]

$$D_x = \frac{kT}{6\pi\eta r_H^x} \quad (4)$$

However, eq 4 is only valid for a hard spherical particle of dimensions much larger than the molecules of the solvent, which is considered as a continuum. When the size of the particle $x$ approaches that of the solvent molecules, the frictional coefficient (i.e., the denominator of eq 4) must be corrected by a factor derived from microfrictional theory[22] and semiempirically improved by Chen and Chen,[23] which eventually yields eq 5, wherein $r_{solv}$ is the hydrodynamic radius of the solvent.

$$D_x = \left(\frac{kT}{6\pi\eta r_H^x}\right)[1 + 0.695(r_{solv}/r_H^x)^{2.234}] \quad (5)$$

Taking $D_{ZnLu2}$ = 5.86(5) × 10$^{-10}$ m$^2$ s$^{-1}$ and $D_{solv}$ = $D_{CHD_2CN}$ = 2.39(5) × 10$^{-9}$ m$^2$ s$^{-1}$ from diffusion-ordered spectroscopic measurements in $CD_3CN$ (diffusion-ordered spectroscopy (DOSY)-NMR at 293 K), we compute $r_{solv}/r_H^x = D_x/D_{solv}$ = 0.245 (eq 4), from which $r_H^{ZnLu2}$ = 10.4(1) Å can be estimated with eq 5 for the pseudospherical hydrodynamic radius of *HHH*-$[ZnLu_2(\mathbf{L5})_3]^{8+}$. Following the suggestion of Lehn and co-workers for the geometrical description of polynuclear double-stranded helicates in solution,[19] *HHH*-$[ZnLu_2(\mathbf{L5})_3]^{8+}$ could be considered as a prolate (i.e., cigar-like) ellipsoid, for which an analytical form of the shape factor $f(p)$ has been derived by Perrin (eq 6, $p = a/b \geq 0$, wherein $a$ and $b$ are respectively the major and minor axes of the ellipsoids).[24] For *HHH*-$[ZnLu_2(\mathbf{L5})_3]^{8+}$, we calculate $f(p)$ = 8.8/10.4 = 0.85 with eq 3, from which a fit with eq 6 eventually gives $p$ = 3.9. Assuming a reasonable maximum diameter for the rigid triple helix defined by twice the Lu1···H23 contact distance (Figures 3 and 4, $b = 2d$(Lu1···H23) = 12.3 Å),

(18) (a) Connolly, M. L. *Science* **1983**, *221*, 709–713. (b) Connolly, M. L. *J. Appl. Crystallogr.* **1983**, *16*, 548–558.
(19) Allouche, L.; Marquis, A.; Lehn, J.-M. *Chem.Eur. J.* **2006**, *12*, 7520–7525.
(20) Candau, S. J. *Surfactant Solutions*; Zana, R., Ed.; Marcel Dekker Inc.: New York, **1987**; pp 157−158.
(21) (a) Einstein, A. *Ann. Phys.* **1906**, *19*, 289–306. (b) Einstein, A. *Ann. Phys.* **1906**, *19*, 371–381. (c) Sharma, M.; Yashonath, S. J. *Phys. Chem. B* **2006**, *110*, 17207–17211.
(22) Gierer, A.; Wirtz, K. Z. *Naturforsch. A: Astrophys., Phys., Phys. Chem.* **1953**, *8*, 532–538.
(23) Chen, H.-C.; Chen, S.-H. *J. Phys. Chem.* **1984**, *88*, 5118–5121.
(24) (a) Perrin, J. *J. Phys. Radium* **1934**, *5*, 497–511. (b) Perrin, J. *J. Phys. Radium* **1936**, *7*, 1–11.

we deduce the length of the long axis of the ellipsoid $a = pb = 3.9 \times 12.3 = 48$ Å, in complete disagreement with a total length of 26.6 Å estimated for *HHH*-$[ZnLu_2(\mathbf{L5})_3]^{8+}$ in the solid state (Figure 3).

$$f(p) = p^{1/3}(p^2-1)^{-1/2}\ln[p + (p^2-1)^{1/2}] \qquad (6)$$

The treatment of a trinuclear palindromic triple helix as a prolate ellipsoid is thus not adequate, and we then considered the semiempirical approach of Garcia De La Torre and co-workers for the specific case of rigid (supra) molecular cylinders with a diameter $\Theta$ and a total length $L$ (eq 7, $p' = L/\Theta$).[25]

$$D_x = \frac{kT(\ln p' + 0.312 + 0.565(p')^{-1} - 0.1(p')^{-2})}{3\pi\eta L} \qquad (7)$$

Neglecting the microfrictional correction, which accounts for less than 3% for the large triple-stranded helicate *HHH*-$[ZnLu_2(\mathbf{L5})_3]^{8+}$ ($0.695(r_{solv}/r_H^x)^{2.234} \leq 0.03$ in eq 5), the application of eq 7 with $\Theta = 12.3$ Å yields $L = 27$ Å and $p' = 2.2$ in very good agreement with the geometrical data obtained in the crystal structure. We can thus safely conclude that the solid-state structure is retained in solution except for some small structural relaxation producing an ideal molecular cylinder on the NMR time scale ($C_3$ symmetry and 27 × 12.3 Å dimensions).

**Following the Self-Assembly Processes of L5 with d- and f-Block Cations in Solution: Homometallic Complexes of L5 with Zn(II).** ESI-MS titrations of $Zn(CF_3SO_3)_2$ into a $10^{-4}$ M solution of **L5** in acetonitrile were performed for metal/ligand ratios in the range 0.33−1.66 (Table S5, Supporting Information). The spectra show the formation of a series of ionic species which evolve with changes in the stoichiometric ratio. For low Zn/**L5** ratios (0.33−0.66), the spectra are dominated by peaks with $m/z$ ratios corresponding to complexes of the type $[Zn(\mathbf{L5})_3(CF_3SO_3)_x]^{(2-x)+}$ and $[Zn(\mathbf{L5})_2(CF_3SO_3)_x]^{(2-x)+}$ ($x = 0, 1$). While the relative intensity of the triple-stranded species $[Zn(\mathbf{L5})_3(CF_3SO_3)_x]^{(2-x)+}$ ($x = 0, 1$) tends to zero for Zn/**L5** > 0.66, peaks for the double-stranded species $[Zn(\mathbf{L5})_2(CF_3SO_3)_x]^{(2-x)+}$ ($x = 0, 1$) remain the most intense for ratios of up to Zn/**L5** = 1. From Zn/**L5** = 1−1.66, peaks corresponding to complexes $[Zn_2(\mathbf{L5})_2(CF_3SO_3)_x]^{(4-x)+}$ ($x = 1-3$), $[Zn_2(\mathbf{L5})_3(CF_3SO_3)_x]^{(4-x)+}$ ($x = 1-3$), $[Zn_3(\mathbf{L5})_2(CF_3SO_3)_x]^{(6-x)+}$ ($x = 1-4$), and even $[Zn_4(\mathbf{L5})_3(CF_3SO_3)_x]^{(8-x)+}$ ($x = 4, 5$) then start to appear, indicating the formation of higher nuclearity complexes.

As a consequence of the interannular conformational changes accompanying metal chelation, the two main envelopes of the $\pi-\pi^*$ transitions in the UV−vis spectrum of **L5** ($\lambda_{max} \approx 230$ and 320 nm) experience bathochromic shifts on coordination of **L5** to metal cations. Analogous titrations to those performed using ESI-MS were thus carried out by monitoring spectral changes in the range $220 \leq \lambda \leq 420$ nm on addition of a solution of $Zn(CF_3SO_3)_2$ ($2 \times 10^{-3}$ M) to **L5** ($2 \times 10^{-4}$ M) in acetonitrile. As is apparent in Figure 5a, sequential aliquots of metal solution cause complex variations in the UV−vis spectra. Clear inflection points can be seen in the plots of $\varepsilon$ versus the Zn/**L5** ratio (Figure 5a) at Zn/**L5** ≈ 0.5, 1, and 1.5. However, evolving factor analysis of the entire data set[26,27] suggests that the spectral variations are due to six absorbing species, and a model which considers the formation of the five complexes characterized by equilibria 8−12 can be satisfyingly fitted to the spectrophotometric data (Figure S1a and S2, Supporting Information).[27] Agreement with the qualitative ESI-MS data is generally good, though attempts to incorporate a triple-stranded bimetallic complex of the type $[Zn_2(\mathbf{L5})_3]^{4+}$ were unsuccessful. This is perhaps not surprising given the low intensity observed for peaks corresponding to this species in the ESI-MS, which suggests that it is present at very low concentrations.

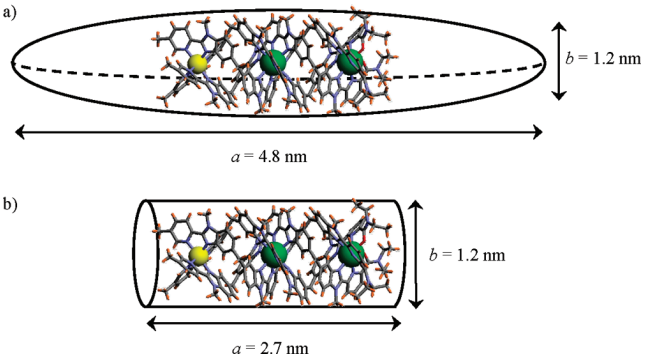


**Figure 4.** Schematic structural models for *HHH*-$[ZnLu_2(\mathbf{L5})_3]^{8+}$ in acetonitrile as deduced from translational autodiffusion coefficients: (a) inadequate rigid prolate ellipsoid and (b) adequate rigid cylinder.

$$3\mathbf{L5} + Zn^{2+} \rightleftharpoons [Zn(\mathbf{L5})_3]^{2+} \quad \log\beta_{1,0,3}^{Zn,Lu,L5} = 22.3(5) \qquad (8)$$

$$2\mathbf{L5} + Zn^{2+} \rightleftharpoons [Zn(\mathbf{L5})_2]^{2+} \quad \log\beta_{1,0,2}^{Zn,Lu,L5} = 17.7(4) \qquad (9)$$

$$2\mathbf{L5} + 2Zn^{2+} \rightleftharpoons [Zn_2(\mathbf{L5})_2]^{4+} \quad \log\beta_{2,0,2}^{Zn,Lu,L5} = 27.0(4) \qquad (10)$$

$$3\mathbf{L5} + 4Zn^{2+} \rightleftharpoons [Zn_4(\mathbf{L5})_3]^{8+} \quad \log\beta_{4,0,3}^{Zn,Lu,L5} = 48.8(6) \qquad (11)$$

$$2\mathbf{L5} + 3Zn^{2+} \rightleftharpoons [Zn_3(\mathbf{L5})_2]^{6+} \quad \log\beta_{3,0,2}^{Zn,Lu,L5} = 33.2(4) \qquad (12)$$

The value of $\log\beta_{1,0,3}^{Zn,Lu,L5} = 22.3(5)$ established for $[Zn(\mathbf{L5})_3]^{2+}$ is identical within error to that obtained for

(25) (a) Tirado, M. M.; Martinez, C. L.; Garcia De La Torre, J. *J. Chem. Phys.* **1984**, *81*, 2047–2052. (b) Hamelin, B.; Jullien, L.; Derouet, C.; Hervé, C.; Berthault, P. *J. Am. Chem. Soc.* **1998**, *120*, 8438–8447.

(26) Malinowski, E. R.; Howery, D. G. *Factor Analysis in Chemistry*; Wiley: New York, **1980**.

(27) (a) Gampp, H; Maeder, M.; Meyer, C. J.; Zuberbuhler, A. D. *Talanta* **1985**, *23*, 1133–1139. (b) Gampp, H; Maeder, M.; Meyer, C. J.; Zuberbuhler, A. D. *Talanta* **1986**, *33*, 943–951.

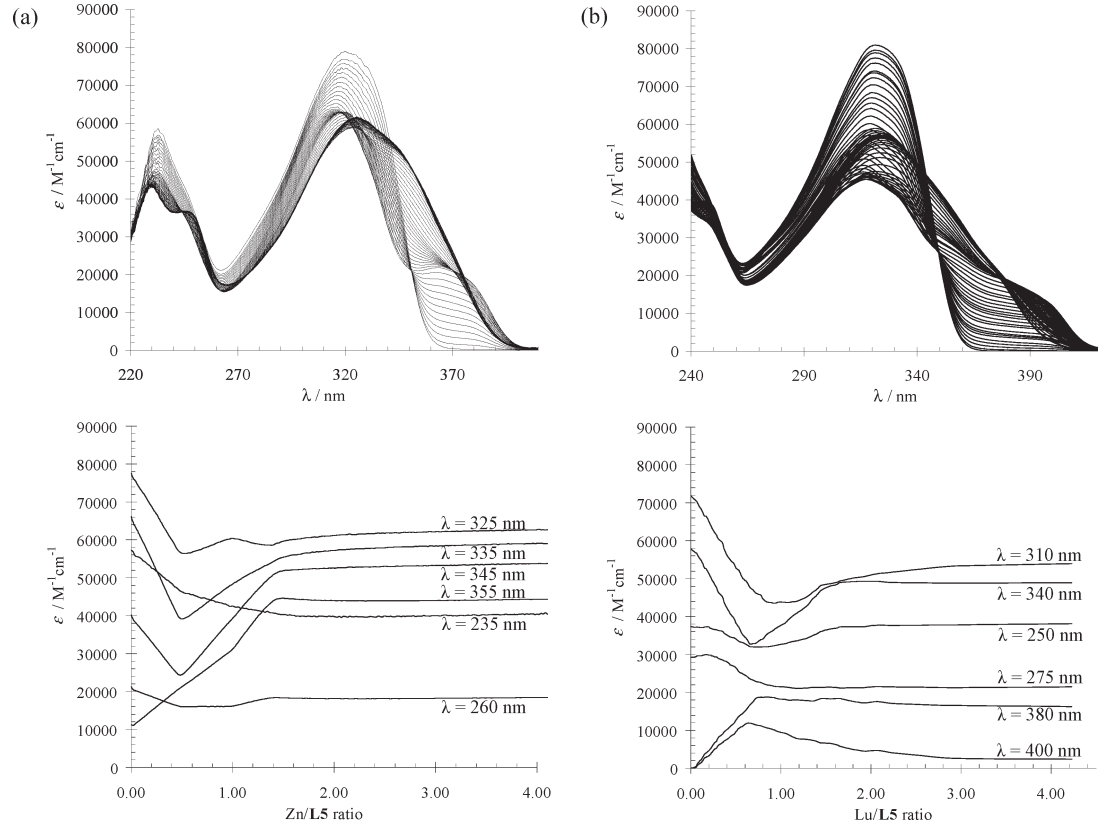


**Figure 5.** Variation of absorption spectra and molar extinction coefficients observed during spectrophotometric titrations of **L5** ($2 \times 10^{-4}$ M) with (a) $Zn(CF_3SO_3)_2$ ($2 \times 10^{-3}$ M) and (b) $Lu(CF_3SO_3)_3$ ($2 \times 10^{-3}$ M) in MeCN + 0.01 M $[Bu_4N](CF_3SO_3)$.

the previously reported complex $[Zn(\mathbf{L2})_3]^{2+}$ (Chart 1, $\log \beta_{1,0,3}^{Zn,Lu,L2} = 22(1)$),[6a] consistent with the Zn(II) ion being octahedrally coordinated by the three $N_2$ sites of **L5**. These values have been further corroborated by analogous titrations of $Zn(CF_3SO_3)_2$ ($10^{-3}$ M) into a solution of the monotopic bidentate ligand **L6** ($10^{-4}$ M, Chart 2 and Figure S3, Supporting Information),[28] for which the spectrophotometric data were successfully modeled by the four absorbing species in equilibria 13−15. Of the three complexes observed for **L6**, only the saturated triple-stranded complex $[Zn(\mathbf{L6})_3]^{2+}$ has been structurally characterized,[28b] and its $\log \beta_{1,0,3}^{Zn,Lu,L6}$ value of 22.7(4) is consistent with the reported quantitative formation of a rapidly exchanging 3:1 mixture of *HHT*-/*HHH*-isomers in $CD_3CN$, as previously observed by $^1$H NMR spectroscopy at 293 K.[28b]

$$3\mathbf{L6} + Zn^{2+} \rightleftharpoons [Zn(\mathbf{L6})_3]^{2+} \quad \log \beta_{1,0,3}^{Zn,Lu,L6} = 22.7(4) \tag{13}$$

$$2\mathbf{L6} + Zn^{2+} \rightleftharpoons [Zn(\mathbf{L6})_2]^{2+} \quad \log \beta_{1,0,2}^{Zn,Lu,L6} = 15.6(3) \tag{14}$$

$$\mathbf{L6} + Zn^{2+} \rightleftharpoons [Zn(\mathbf{L6})]^{2+} \quad \log \beta_{1,0,1}^{Zn,Lu,L6} = 7.8(2) \tag{15}$$

(28) (a) Charbonnière, L. J.; Williams, A. F.; Piguet, C.; Bernardinelli, G.; Rivera-Minten, E. *Chem.Eur. J.* **1998**, *4*, 485. (b) Torelli, S.; Delahaye, S.; Hauser, A.; Bernardinelli, G.; Piguet, C. *Chem.Eur. J.* **2004**, *10*, 3503–3516.

$^1$H NMR spectra were recorded for selected Zn/**L5** ratios in order to examine the structures of the complexes participating in equilibria 8−12 (Figure S4, Supporting Information). Poor ligand solubility prevented the use of pure $CD_3CN$ for ratios in the range 0.33−0.66 (at the desired NMR concentration of $1.5 \times 10^{-2}$ M), and so a 2:1 mixture of $CD_3CN/CDCl_3$ was used. The spectra are by and large broadened by exchange processes and complicated by the presence of numerous low-symmetry species, impeding structural assignment. Several features are, however, worth noting. For Zn/**L5** ratios of 0.33−0.66, the $^1$H NMR spectra are dominated by one species whose end point appears at a 1:2 Zn/**L5** stoichiometry (Figure S4b, Supporting Information). Signal overlap precludes a thorough peak-to-proton assignment, but a structure may nonetheless be proposed in which one Zn(II) ion is octahedrally coordinated by the central $N_3$ donor sets of two strands of **L5** in a *cc*-$[Zn(\mathbf{L5})_2]^{2+}$ complex (*c* = central binding site). Reasoning for this includes the observations that (i) only one set of ligand peaks is present, indicating that the two ligand strands are related by $C_2$ symmetry on the NMR time scale, and (ii) two low closely spaced singlets, tentatively assigned to $H^9$ and $H^{17}$ (numbering in Figure 1a), appear in the range $5.8 \leq \delta \leq 6.0$ ppm typically associated with interstrand aromatic shielding effects. The first point implies a head-to-head (*HH*) orientation of the two strands, with Zn(II) lying in either of the three successive $N_4$, $N_6$, or $N_4O_2$ coordination sites. The second point rules out the possibity of the Zn(II) ion occupying a terminal site because only ***one*** shielded singlet would be detected at low frequency in this case (assigned either to $H^6$ ($N_4$ site)

or to $H^{20}$ ($N_4O_2$ site)). On further addition of Zn(II) to **L5** (Figure S4c−f, Supporting Information), the spectra become uninterpretable due to the expected co-existence of numerous low-symmetry microspecies undergoing exchange on the NMR time scale (Figure S2, Supporting Information).

**Homometallic Complexes of L5 with Lu(III).** ESI-MS titrations of $Lu(CF_3SO_3)_3$ into a $10^{-4}$ M solution of **L5** in acetonitrile ($0.33 \leq Lu/\mathbf{L5} \leq 1.66$) again show a complex evolution of ionic species with an increasing Lu/**L5** ratio (Table S6, Supporting Information). For low Lu/**L5** ratios (0.33−0.66), the spectra are dominated by peaks with $m/z$ ratios corresponding to complexes of the type $[Lu(\mathbf{L5})_3(CF_3SO_3)_x]^{(3-x)+}$ ($x$ = 0, 1) and $[Lu_2(\mathbf{L5})_3(CF_3SO_3)_x]^{(6-x)+}$ ($x$ = 1−4), the latter of which can be detected with up to 1.33 equiv of Lu(III) present. Above Lu/**L5** = 1, peaks corresponding to higher-nuclearity complexes $[Lu_3(\mathbf{L5})_3(CF_3SO_3)_x]^{(9-x)+}$ ($x$ = 3−6), $[Lu_2(\mathbf{L5})_2(CF_3SO_3)_x]^{(6-x)+}$ ($x$ = 3, 4), and $[Lu_3(\mathbf{L5})_2(CF_3SO_3)_x]^{(9-x)+}$ ($x$ = 5−7) gain in relative intensity. The titrations were followed in parallel by batch spectrophotometry (Figure 5b), and variations in the UV−vis spectra of **L5** observed upon the addition of Lu $(CF_3SO_3)_3$ ($2 \times 10^{-3}$ M) to a solution of **L5** ($2 \times 10^{-4}$ M) in acetonitrile were modeled with five absorbing species according to equilibria 16−19. Despite the inherent error associated with the batch method, the multi non-linear least-squares fitting procedure converges to a stable minimum and yields chemically sensible calculated absorption spectra (Figures S1b and S5, Supporting Information).

$$3\mathbf{L5} + Lu^{3+} \rightleftharpoons [Lu(\mathbf{L5})_3]^{3+} \quad \log \beta_{0,1,3}^{Zn,Lu,L5} = 16.7(2) \tag{16}$$

$$3\mathbf{L5} + 2Lu^{3+} \rightleftharpoons [Lu_2(\mathbf{L5})_3]^{6+} \quad \log \beta_{0,2,3}^{Zn,Lu,L5} = 24.2(3) \tag{17}$$

$$3\mathbf{L5} + 3Lu^{3+} \rightleftharpoons [Lu_3(\mathbf{L5})_3]^{9+} \quad \log \beta_{0,3,3}^{Zn,Lu,L5} = 29.6(4) \tag{18}$$

$$2\mathbf{L5} + 3Lu^{3+} \rightleftharpoons [Lu_3(\mathbf{L5})_2]^{9+} \quad \log \beta_{0,3,2}^{Zn,Lu,L5} = 23.4(2) \tag{19}$$

The cumulative stability constants for $[Lu(\mathbf{L5})_3]^{3+}$ ($\log \beta_{0,1,3}^{Zn,Lu,L5} = 16.7(2)$) and $[Lu_2(\mathbf{L5})_3]^{6+}$ ($\log \beta_{0,2,3}^{Zn,Lu,L5} = 24.2(3)$) compare with those previously reported for complexes $[Lu(\mathbf{L10})_3]^{3+}$ ($\log \beta_{0,1,3}^{Zn,Lu,L10} = 17.1(5)$),[14b] $[Lu_2(\mathbf{L10})_3]^{6+}$ ($\log \beta_{0,2,3}^{Zn,Lu,L10} = 25.4(5)$),[14b] and $[Lu_2(\mathbf{L11})_3]^{6+}$ ($\log \beta_{0,2,3}^{Zn,Lu,L11} = 25.5(1)$)[15] based on ligands **L10** and **L11**, respectively (Chart 2). In particular, relatively small differences in stability between the $[Lu_2(\mathbf{L}\phi)_3]^{6+}$ ($\phi$ = 5, 10, 11) complexes highlight the marginal impact of varying the donor motifs from a saturated all-$N_2O$ structure, as exemplified by $[Lu_2(\mathbf{L10})_3]^{6+}$, to the mixed $N_2O$- and $N_3$-donor sets in $[Lu_2(\mathbf{L5})_3]^{6+}$ and $[Lu_2(\mathbf{L11})_3]^{6+}$.

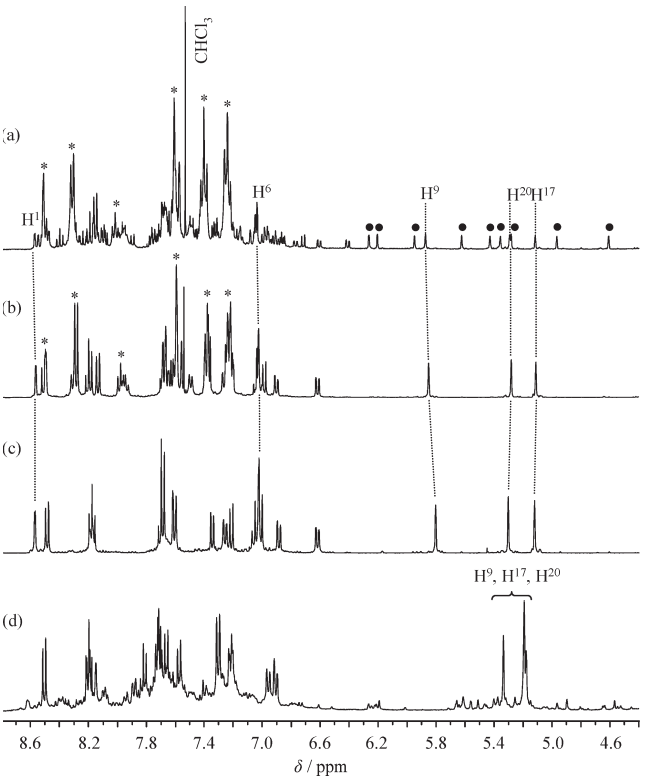


**Figure 6.** Aromatic region of the 400 MHz $^1$H NMR spectra for solutions containing $Lu(CF_3SO_3)_3$ and **L5** ($|\mathbf{L5}|_{tot} = 1.5 \times 10^{-2}$ M) with Lu/**L5** ratios of (a) 0.33 (selected proton resonances of *HHH*-$[Lu_2(\mathbf{L5})_3]^{6+}$ labeled; the symbol ● denotes $H^9$, $H^{17}$, and $H^{20}$ in *HHT*-$[Lu_2(\mathbf{L5})_3]^{6+}$), (b) 0.33 (after 24 h), (c) 0.66 (after 24 h), and (d) 1.0 (after 24 h). The spectra of solutions a and b were recorded in a 2:1 $CD_3CN/CDCl_3$ mixture, while spectra c and d were recorded in pure $CD_3CN$. An asterisk denotes free **L5**.

The $^1$H NMR spectrum of a solution containing a 1:3 ratio of Lu/**L5** ($|\mathbf{L5}|_{tot} = 1.5 \times 10^{-2}$ M, Figure 6a) shows multiple species interchanging slowly on the NMR time scale. On equilibrating for 24 h, the spectrum simplifies considerably (Figure 6b), and two dominant sets of peaks can be identified as originating from the non-complexed ligand and another highly symmetric species. The latter displays one set of peaks for protons in **L5**, with all methylene $-CH_2-$ groups appearing as AB spin systems, as for the diastereotopic methylene protons in *HHH*-$[ZnLu_2(\mathbf{L5})_3]^{8+}$. The addition of one more equivalent of Lu(III), followed by equilibration, causes no further change other than the total disappearance of peaks due to a free ligand, implying an end-point Lu/**L5** stoichiometry of 2:3 for the observed complex (Figure 6c). This composition is supported by the intense peaks for cations $[Lu_2(\mathbf{L5})_3(CF_3SO_3)_x]^{(6-x)+}$ ($x$ = 1−4) detected for ratios in the range $0.33 \leq Lu/\mathbf{L5} \leq 1.66$ during ESI-MS titrations. Close scrutiny of the (one- and two-dimensional) $^1$H NMR spectra of the species formed under these conditions points conclusively to a $C_3$-symmetric helicate structure in which, remarkably, three co-aligned strands of **L5** coordinate two Lu(III) ions via the terminal $N_2O$ and central $N_3$ sites (Table 1). The resulting complex *HHH*-$[Lu_2(\mathbf{L5})_3]^{6+}$ thus presents a vacant terminal $N_6$ binding site comprised of the three non-bound bidentate units of **L5**. NOE effects associated with the interannular trans−trans to cis−cis conformational changes occurring

on metal complexation are observed exclusively for proton pairs $H^{12}/Me^3$, $H^{14}/Me^4$, and $H^{23}/Me^5$ (numbering in Figure 1a), which are localized on the benzimidazole–pyridyl segments constituting the tridentate $N_3$ and $N_2O$ chelates. That no NOE effects are detected for protons $H^3/Me^2$ confirms the retention of a trans–trans conformation for the bidentate unit and precludes its being coordinated to a metal. Likewise, interstrand through-space NOE effects are observed only for $H^5/Me^3$ and $H^{21}/Me^4$ where metal coordination ensures tight helical wrapping of the three ligands about the helical axis. The complex *HHH*-$[Lu_2(\mathbf{L5})_3]^{6+}$ gives rise to three resonances ($H^9$, $H^{17}$, and $H^{20}$, Table 1) in the region typically associated with the shielded aromatic protons of the helicate structure ($5.0 \leq \delta \leq 5.9$ ppm). Proton $H^6$ ($\delta$ 6.90 ppm) does not resonate at a low frequency since the noncomplexed bidentate unit is sufficiently mobile to adopt conformations other than those in which $H^6$ is subjected to the ring current anisotropies of the aromatic heterocycles on the adjacent strands of **L5**.

The remaining peaks present in the $^1$H NMR spectra of pre-equilibrated solutions containing either a 1:3 ratio of Lu/**L5** (Figure 6a) or a 2:3 ratio of Lu/**L5** (Figure S6, Supporting Information) can now be reasonably assigned to the isomeric $C_1$-symmetric complex *HHT*-$[Lu_2(\mathbf{L5})_3]^{6+}$, in which one of the three ligand strands is aligned in an antiparallel fashion with respect to the other two. Nine singlets appear for this species in the shielded aromatic region ($4.5 \leq \delta \leq 6.3$ ppm, Figure 6a), consistent with protons $H^9$, $H^{17}$, and $H^{20}$ each occupying unique chemical environments on the three different ligand strands. Assignment of these peaks to the structural isomer *HHT*-$[Lu_2(\mathbf{L5})_3]^{6+}$ is also in keeping with the calculated speciation diagram for $|\mathbf{L5}|_{tot} = 0.01$ M, which predicts quantitative assembly of $[Lu_2(\mathbf{L5})_3]^{6+}$ for the ratio Lu/**L5** = 0.66 (Figure S5, Supporting Information), and the exclusive detection of cations with $m/z$ values corresponding to $[Lu_2(\mathbf{L5})_3(CF_3SO_3)_x]^{(6-x)+}$ ($x = 1-4$) by ESI-MS at this ratio (Table S6, Supporting Information). The gradual disappearance of peaks for *HHT*-$[Lu_2(\mathbf{L5})_3]^{6+}$ to give pure *HHH*-$[Lu_2(\mathbf{L5})_3]^{6+}$ over ca. 24 h (Figure S6, Supporting Information) thus constitutes a thermodynamic resolution of the *HHH* isomer from an initial kinetic 3:1 distribution of the *HHT*/*HHH* isomers according to eq 20.

$$HHT\text{-}[Lu_2(\mathbf{L5})_3]^{6+} \underset{k_{HHH}}{\overset{k_{HHT}}{\rightleftharpoons}} HHH\text{-}[Lu_2(\mathbf{L5})_3]^{6+}$$

$$K_{iso} = \frac{k_{HHT}}{k_{HHH}} \qquad (20)$$

That the *HHH*-isomer is the only species detected at equilibrium implies that it is stabilized well beyond the statistical entropic contribution for which a final equilibrium constant of $K_{iso}^{stat} = 3$, in favor of the *HHT* isomer, would be anticipated.[29] If the limit of detection by NMR of the *HHT* isomer is fixed at ca. 1%, we calculate from eq 20 that $K_{iso} \geq 99$, and thus the free energy of isomerization amounts to $\Delta G_{iso}^0 \leq -11.4$ kJ mol$^{-1}$. Under these conditions, we can set $k_{HHT} \geq 99k_{HHH}$ for the rate constants characterizing the exchange process, and the time-dependent concentrations of *HHT* and *HHH* conform to the simple first-order eqs 21 and 22, respectively.[30]

$$|HHT|_t = |HHT|_0 \, e^{(-k_{HHT} \cdot t)} \qquad (21)$$

$$|HHH|_t = |HHH|_0 - |HHT|_0 \cdot e^{(-k_{HHT} \cdot t)} \qquad (22)$$

The plot of $\ln|HHH|_t$ versus time is indeed linear (Figure S7, Supporting Information), and from its slope we estimate $k_{HHT}^{295} = 3.94 \times 10^{-5}$ s$^{-1}$, with a corresponding half-life for the *HHT* isomer of $\tau_{HHT}^{295} = \ln(2)/k_{HHT}^{295} = 4.89$ h, a kinetic parameter which justifies the need to leave solutions containing in situ prepared polymetallic lanthanide complexes to equilibrate for at least 24 h. DOSY-NMR of the stable *HHH*-$[Lu_2(\mathbf{L5})_3]^{6+}$ isomer gives $D_{Lu2} = 6.26(3) \times 10^{-10}$ m$^2$ s$^{-1}$ in acetonitrile at 293 K, a value slightly larger than that found for *HHH*-$[ZnLu_2(\mathbf{L5})_3]^{8+}$ because of the removal of Zn(II) and the loss in rigidity of the extremity of the triple-stranded helix. Application of eq 7 with the same fixed diameter $\Theta = 12.3$ Å yields $L = 23$ Å, which resumes to a 14% contraction of the length of the cylinder on going from *HHH*-$[ZnLu_2(\mathbf{L5})_3]^{8+}$ ($L = 2.7$ nm) to *HHH*-$[Lu_2(\mathbf{L5})_3]^{6+}$ ($L = 2.3$ nm). On increasing the Lu/**L5** ratio to 1:1 and equilibrating for 36 h (Figure 6d), the spectrum obtained still shows one predominant species in solution, the number of proton resonances of which suggests the retention of high symmetry. Some of the diagnostic features for a triple-stranded helicate structure (low field singlets, diastereotopic methylene resonances, etc.) are still present, and it is plausible that a $C_3$-symmetric *HHH*-$[Lu_3(\mathbf{L5})_3]^{9+}$ complex has formed, in keeping with the formulation $[Lu_3(\mathbf{L5})_3]^{9+}$ anticipated from ESI-MS and UV–vis titrations (Figure S5, Supporting Information). Assignment of the peaks and confirmation of the proposed structure is, however, obscured by the appearance of numerous low-intensity peaks, which suggest the presence of at least one more complex in solution, such as $[Lu_3(\mathbf{L5})_2]^{9+}$ postulated in equilibrium 19 (Figure S5, Supporting Information).

**Heteropolymetallic Complexes of L5 with Lu(III) and Zn(II).** ESI-MS titrations of a 1:2 mixture of $Zn(CF_3SO_3)_2$ and $Lu(CF_3SO_3)_3$ ($|M|_{tot} = |Zn|_{tot} + |Lu|_{tot} = 10^{-3}$ M) into a solution of **L5** ($|\mathbf{L5}|_{tot} = 10^{-4}$ M) in acetonitrile were performed for $M_{tot}$/**L5** ratios in the range 0.33–1.66. All spectra show significant quantities of the bimetallic helicate *HHH*-$[ZnLu_2(\mathbf{L5})_3]^{8+}$, with peaks occurring at $m/z$ 464.2, 566.4, 709.7, 924.1, and 1282.0 corresponding to the series of complex cations $[ZnLu_2(\mathbf{L5})_3(CF_3SO_3)_x]^{(8-x)+}$ ($x = 1-5$, Table S7, Supporting Information). For ratios $M_{tot}/\mathbf{L5} < 1.00$, peaks due to free ligands and complexes $[Zn(\mathbf{L5})_2]^{2+}$ and $[Lu(\mathbf{L5})_3]^{3+}$ are also present, indicative of competition for lower-nuclearity homometallic species. Conversely, for the range $1.33 \leq M_{tot}/\mathbf{L5} \leq 1.66$, the spectra show intense peaks at $m/z$ 478.0, 603.2, 791.4, 1104.7, and 1731.9 due to a series of

(29) Ercolani, G.; Piguet, C.; Borkovec, M.; Hamacek, J. *J. Phys. Chem. B* **2007**, *111*, 12195–12203.

(30) Starzak, M. E. In *Mathematical Methods in Chemistry and Physics*; Plenum: New York, **1989**; Chapter 6, p 289.

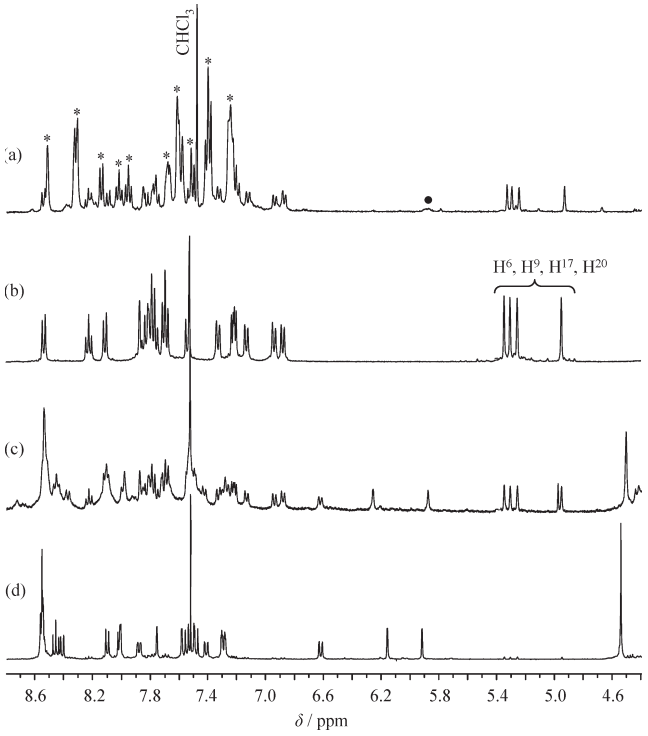


**Figure 7.** Aromatic region of the 400 MHz $^1$H NMR spectra for solutions containing a 1:2 mixture of $Zn(CF_3SO_3)_2$ and $Lu(CF_3SO_3)_3$ and **L5** ($|\mathbf{L5}|_{tot} = 1.5 \times 10^{-2}$ M) with $M_{tot}/\mathbf{L5}$ ratios of (a) 0.33 ($|Zn|_{tot}/|Lu|_{tot}/|\mathbf{L5}|_{tot}$ = 1:2:9, an asterisk denotes free **L5**, and the symbol ● denotes *cc*-$[Zn(\mathbf{L5})_2]^{2+}$), (b) 1.00 ($|Zn|_{tot}/|\mathbf{Lu}|_{tot}/|\mathbf{L5}|_{tot}$ = 1:2:3), and (c) 1.66 ($|Zn|_{tot}/|\mathbf{Lu}|_{tot}/|\mathbf{L5}|_{tot}$ = 5:10:9). Spectrum d was obtained for $|Zn|_{tot}/|\mathbf{Lu}|_{tot}/|\mathbf{L5}|_{tot}$ = 1:1:1). All spectra were recorded in a 2:1 $CD_3CN/CDCl_3$ mixture.

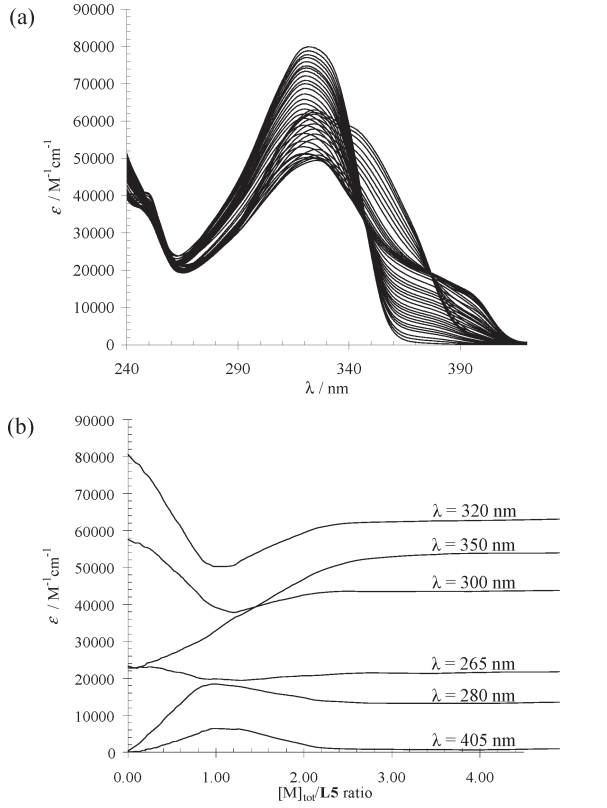


**Figure 8.** Variation of absorption spectra and molar extinction coefficients observed during batch spectrophotometric titrations of **L5** ($2 \times 10^{-4}$ M) with a solution containing a 1:2 mixture of $Zn(CF_3SO_3)_2$ ($0.33 \times 10^{-3}$ M) and $Lu(CF_3SO_3)_3$ ($0.66 \times 10^{-3}$ M) in MeCN and 0.01 M $[Bu_4N](CF_3SO_3)$.

triflate adducts with $[Zn_2Lu_2(\mathbf{L5})_2(CF_3SO_3)_x]^{(10-x)+}$ ($x$ = 4−8) formulations. Other bimetallic species such as $[ZnLu_2(\mathbf{L5})_2]^{8+}$ and $[Zn_2Lu(\mathbf{L5})_2]^{7+}$ are also detectable, but with only low relative intensities.

The $^1$H NMR spectra recorded for solutions containing $M_{tot}/\mathbf{L5}$ ratios in the range 0.33−1.66 ($|\mathbf{L5}|_{tot} = 1.5 \times 10^{-2}$ M) reflect a number of these observations (Figure 7). Signals due to *HHH*-$[ZnLu_2(\mathbf{L5})_3]^{8+}$ systematically increase in intensity as the stoichiometric ratio $M_{tot}/\mathbf{L5}$ = 1.00 ($|Zn|_{tot}/|Lu|_{tot}/|\mathbf{L5}|_{tot}$ = 1:2:3 in Figure 7) is approached, then attenuate on the further addition of metal. Likewise, for low ratios of $M_{tot}/\mathbf{L5} < 0.66$, the spectra show abundant peaks due to free ligands and several baseline signals, one of which can be identified as the two closely spaced singlets ($5.8 \le \delta \le 6.0$ ppm) of *cc*-$[Zn(\mathbf{L5})_2]^{2+}$ (Figure 7a). Interestingly, at ratios of $M_{tot}/\mathbf{L5} >$ 1.00, peaks due to *HHH*-$[ZnLu_2(\mathbf{L5})_3]^{8+}$ are equaled in intensity by those of another species (Figure 7c), for which parallel titrations of a 1:1 mixture of $Zn(CF_3SO_3)_2$ and $Lu(CF_3SO_3)_3$ into a solution of **L5** ($|\mathbf{L5}|_{tot} = 10^{-4}$ M) indicate a clear end-point Lu/Zn/**L5** stoichiometry of 1:1:1. The $^1$H NMR spectrum of this solution shows one major species (Figure 7d), displaying a single set of peaks for **L5**, compatible with the formation of a $C_2$-symmetric $[Zn_2Lu_2(\mathbf{L5})_2]^{10+}$ complex, as observed in the ESI-MS. Unlike the saturated helicates *HHH*-$[ZnLu_2(\mathbf{L5})_3]^{8+}$ and *HHH*-$[Lu_2(\mathbf{L5})_3]^{6+}$, however, all four pairs of methylene protons ($H^{7,8}$, $H^{18,19}$, $H^{26,27}$, and $H^{28,29}$) in $[Zn_2Lu_2(\mathbf{L5})_2]^{10+}$ appear enantiotopic. Given that these singlets do broaden substantially on reducing the temperature to 248 K, we can reasonably conclude that the incriminated complex is sufficiently fluctional to render the methylene protons chemically equivalent on the NMR time scale at 295 K, as previously reported for $[Ln_2(\mathbf{L10})_2]^{6+}$.[14b]

The variations in the extinction coefficient (in the range $220 \le \lambda \le 420$ nm) observed during batch spectrophotometric titrations cease to evolve after a ratio of $M_{tot}/\mathbf{L5}$ = 3 has been attained (Figure 8). An evolving factor analysis suggests the participation of at least six absorbing species, but a model incorporating more than five combinations of competing homo- (equilibria 8−12 and 16−19) and heteropolymetallic complexes did not reach convergence. A simultaneous fit of all spectrophotometric data (i.e., a global analysis of the titration data for all three systems) was therefore attempted by introducing fixed cumulative formation constants for those homometallic complexes predicted to occur at sufficiently high concentrations to be detected above the noise level (see Figure 9, and Figures S2 and S5, Supporting Information) and adjusting only the log $\beta_{1,2,3}^{Zn,Lu,L5}$ and log $\beta_{2,2,2}^{Zn,Lu,L5}$ values associated with equilibria 23 and 24.[31] Fits based on this simplified model reached an acceptable level of convergence and yielded chemically sensible absorption spectra for all components considered. High correlation between the

(31) The global analysis was performed using an in-house-built program in MATLAB which implements the Newton−Gauss nonlinear least-squares fitting algorithm. For details, see: (a) Maeder, M.; Neuhold, Y.-M. In *Practical Data Analysis in Chemistry*; Rutan, S., Walczak, B. Eds.; Elsevier Publishing Co.: Amsterdam, **2007**.

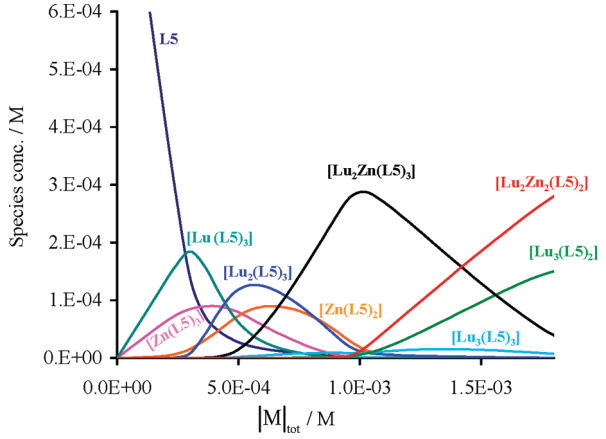


**Figure 9.** Calculated species distribution curve for complexes of **L5** with Zn(II) and Lu(III) for total ligand concentrations of $|\mathbf{L5}|_{tot} = 10^{-3}$ M; $|M|_{tot} = |Zn|_{tot} + |Lu|_{tot}$ and $|Lu|_{tot} = 2|Zn|_{tot}$ (only species contributing to ≥5% of the total distribution are labeled).

latter, in addition to the fact that the model neglects the formation of other heteropolymetallic complexes (such as those detected by ESI-MS), somewhat reduces the reliability of the fitted cumulative stability constants, and so the values reported below are only estimates. We note, however, that the values obtained reasonably predict near-quantitative (>95%) formation of $[ZnLu_2(\mathbf{L5})_3]^{8+}$ at its respective stoichiometric ratio for the millimolar concentration range (Figure 9), as anticipated from both the $^1$H NMR and ESI-MS data. Indeed, a value of $\log \beta_{1,2,3}^{Zn,Lu,L5} < 34.5$ would result in significant quantities of competing homometallic complexes, even at the appropriate Lu/Zn/**L5** stoichiometry of 2:1:3. In light of this, the fitted value of $\log \beta_{1,2,3}^{Zn,Lu,L5} = 36(1)$ is entirely realistic.

$$3\mathbf{L5} + 2Lu^{3+} + Zn^{2+} \rightleftharpoons [ZnLu_2(\mathbf{L5})_3]^{8+} \quad \log \beta_{1,2,3}^{Zn,Lu,L5} = 36(1) \qquad (23)$$

$$2\mathbf{L5} + 2Lu^{3+} + 2Zn^{2+} \rightleftharpoons [Zn_2Lu_2(\mathbf{L5})_2]^{10+} \quad \log \beta_{2,2,2}^{Zn,Lu,L5} = 40(1) \qquad (24)$$

## Conclusion

The considerable number of homometallic complexes formed between the segmental 2−3−3 ligand **L5** and Zn(II) (five identified complexes) or Lu(III) (four identified complexes) contrasts with the detection of only two major heterometallic species *HHH*-$[ZnLu_2(\mathbf{L5})_3]^{8+}$ and $[Zn_2Lu_2(\mathbf{L5})_2]^{10+}$ (Figure 10). This demonstrates that **L5** is judiciously designed for the selective recognition of a 3d−4f−4f sequence of metals, whose stereochemical preferences match the scaffold (one octahedral and two tricapped trigonal prismatic sites) produced by the (*HHH*-) wrapping of three parallel ligands about the helical axis. Among the 11 identified complexes for the Zn(II)/Lu(III)/**L5** system, only three exist as rigid microspecies which can be unambigously characterized in solution by NMR: the $C_2$-symmetrical double-stranded complex *HH*-$[Zn(\mathbf{L5})_2]^{2+}$, in which the metal is pseudo-octahedrally coordinated by the central $N_3$ sites of the ligands, and the two $C_3$-symmetrical helicates *HHH*-$[Lu_2(\mathbf{L5})_3]^{6+}$ and *HHH*-$[ZnLu_2(\mathbf{L5})_3]^{8+}$ (Figure 10). Moreover, the crystal structure of *HHH*-$[ZnLu_2(\mathbf{L5})_3]^{8+}$ evidences intermetallic contact distances close to 9 Å, which strictly correspond to those reported for the hetero- and homometallic complexes previously characterized with ligands **L2**, **L9**−**L12**, a prerequisite for combining all thermodynamic data in a forthcoming global analysis. The stability constants obtained for these three structurally characterized complexes are obviously amenable to being modeled with the site binding model,[12] but $[Zn(\mathbf{L5})_3]^{2+}$ and $[Lu(\mathbf{L5})_3]^{3+}$ can also be useful if they are considered as macrospecies. The thermodynamic and partial NMR data collected for $[Zn(\mathbf{L5})_3]^{2+}$ closely resemble those obtained for the model complex $[Zn(\mathbf{L6})_3]^{2+}$, which exists as a mixture of rapidly interconverting *HHH* ↔ *HHT* isomers on the NMR time scale. Because of the restricted coordination number of Zn(II) (CN ≤ 6), we can reasonably conclude that only the bidentate binding units of **L5** interacts with the metal in $[Zn(\mathbf{L5})_3]^{2+}$, which thus also exists as a mixture of two contributing microspecies *HHH*-$[Zn(\mathbf{L5})_3]^{2+}$ ($C_3$ symmetry) and *HHT*-$[Zn(\mathbf{L5})_3]^{2+}$ ($C_1$ symmetry), both being easily addressed with the site binding model. For $[Lu(\mathbf{L5})_3]^{3+}$, the situation is slightly more complicated with the consideration of eight contributing microspecies depending on the nature of the $N_3$ or $N_2O$ tridentate binding site bound to the metal, but thermodynamic modeling remains accessible.

In this context, the exceptional stability of the unsaturated homometallic helicate *HHH*-$[Lu_2(\mathbf{L5})_3]^{6+}$ escapes rationalization without a more detailed analysis of the microscopic thermodynamic parameters, but the preferred formation of nine-coordinate sites with local 3-fold symmetries ($N_9$ and $N_6O_3$ for *HHH*-$[Lu_2(\mathbf{L5})_3]^{6+}$ compared with $N_8O$ and $N_7O_2$ for HHT-$[Lu_2(\mathbf{L5})_3]^{6+}$) is reminiscent of previous unexplained stabilization observed for binuclear *HHH* triple-stranded lanthanide helicates with unsymmetrical bis-tridentate ligands.[32] Whatever the origin of this stabilization, the subsequent transformation of *HHH*-$[Lu_2(\mathbf{L5})_3]^{6+}$ into *HHH*-$[ZnLu_2(\mathbf{L5})_3]^{8+}$ can be conceptually understood as the addition of the terminal Zn(II) cation without peturbing the coordination of the 4f-block ions. Though naive at first sight, this point of view is substantiated by the translational autodiffusion coefficients which indicate that (i) the cylindrical shape is retained in both complexes and (ii) the total length of the cylinder is increased by 14% upon the addition of Zn(II). Thanks to the five additional thermodynamic formation constants associated with the structurally characterized macrospecies $[Zn(\mathbf{L5})_3]^{2+}$, $[Zn(\mathbf{L5})_2]^{2+}$, $[Lu(\mathbf{L5})_3]^{3+}$, $[Lu_2(\mathbf{L5})_3]^{6+}$, and $[ZnLu_2(\mathbf{L5})_3]^{8+}$, we are now in a position to extract the microscopic parameters controlling the global multicomponent assembly of triple-stranded helicates with ligands **L1**, **L2**, and **L5**−**L12** without resorting to Coulombic constraints.

## Experimental Section

Chemicals were purchased from Fluka AG and Aldrich and used without further purification unless otherwise stated. Starting synthons **1**,[6a] **2**,[17] and ligand **L6**[28] were prepared according to literature procedures. The trifluoromethanesulfonate salt

(32) (a) Jensen, T. B.; Scopelliti, R.; Bunzli, J.-C. G. *Inorg. Chem.* **2006**, *45*, 7806–7814. (b) Jensen, T. B.; Scopelliti, R.; Bunzli, J.-C. G. *Chem.Eur. J.* **2007**, *13*, 8404–8410.

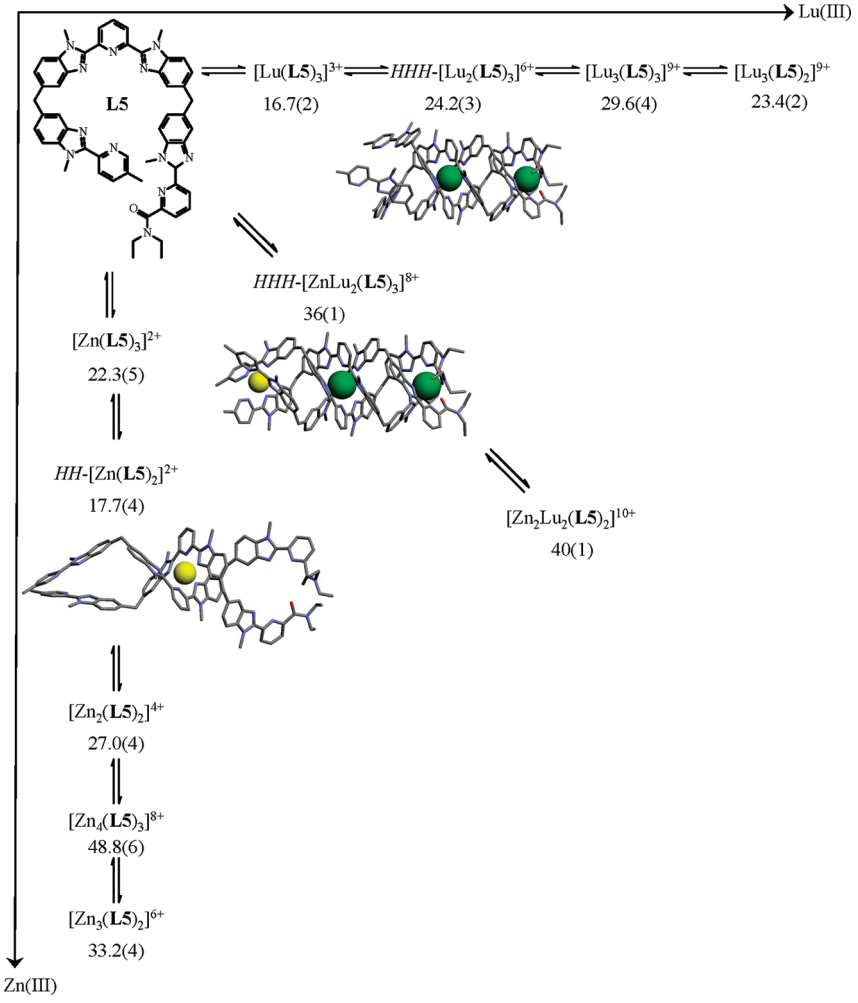


**Figure 10.** Summary of the assembly of **L5** with Zn(II) and Lu(III) in acetonitrile solution. The numerical values correspond to the cumulative formation constants of each complex $[Zn_\alpha Lu_\beta(\mathbf{L5})_\gamma]^{(2\alpha+3\beta)+}$ (log $\beta^{Zn,Ln,L5}_{\alpha,\beta,\gamma}$). The three schematic structures correspond to those complexes fully characterized in solution by NMR (green sphere = Lu(III), yellow sphere = Zn(II)).

$Lu(CF_3SO_3)_3 \cdot xH_2O$ was prepared from the corresponding oxide (Aldrich, 99.99%).[33] The Lu content of a solid salt was determined by complexometric titrations with Titriplex III (Merck) in the presence of urotropine and xylene orange.[34] Acetonitrile and dichloromethane were distilled over calcium hydride. Silicagel plates Merck 60 $F_{254}$ were used for thin layer chromatography (TLC), and Fluka silica gel 60 (0.04−0.063 mm) or Acros neutral activated alumina (0.050−0.200 mm) was used for preparative column chromatography.

**Preparation of 3.** To a solution of the acid derivative **2** (1.2 g, 2.46 mmol, Scheme 1) in dry $CH_2Cl_2$ (30 mL) was added $SOCl_2$ (26.8 mL, 369 mmol) and 3−4 drops of *N*,*N*-dimethylformamide. The resulting suspension was stirred at reflux under $N_2$ for 2 h before removing the solvent and drying the resulting white residue in vacuo for a further 2 h. A solution containing the dinitro derivative **1** (1.3 g, 4.92 mmol, Scheme 1) and $^i Pr_2EtN$ (0.84 mL, 4.92 mmol) in dry $CH_2Cl_2$ (70 mL) was then added carefully under $N_2$, and the solution stirred at reflux for 15 h. On cooling, the reaction mixture was poured into $CH_2Cl_2$ (100 mL) and washed twice with 2 × 50 mL portions of a half-saturated solution of $NH_4Cl_{(aq)}$. The combined organic phases were dried over $Na_2SO_4$, and the solvent was removed under reduced pressure to give a dark brown oil. The crude material was then purified by column chromatography on $SiO_2$ (3% MeOH in $CH_2Cl_2$) to give **3** as a light brown waxy solid (1.65 g, 67%). $^1H$ NMR ($CDCl_3$; 400 MHz): $\delta$ 8.48 (s, Ar−CH), 8.21 (m, Ar−CH), 8.13 (m, Ar−CH), 7.41−8.00 (m, Ar−H), 6.97−7.36 (m, Ar−H), 6.75 (m, Ar−H), 6.57 (m, Ar−H), 4.04−4.44 (m, N−$CH_3$), 2.83−3.96 (m, −$CH_2$−), 2.38 (s, Ar−$CH_3$), 1.00−1.32 (m, −$CH_3$), 0.85 (m, −$CH_3$). Elem anal. calcd (%) for $C_{55}H_{50}N_{12}O_7 \cdot 1.60H_2O$: C, 64.71; H, 5.26; N, 16.46. Found: C, 64.72; H, 5.18; N, 16.40. ESI-MS *m*/*z*: 991.7 $\{[M + H]^+\}$.

**Preparation of L5.** To a solution containing the dinitro derivative **3** (1.0 g, 1.01 mmol) in ethanol/water (300/75 mL) were added activated Fe powder (1.7 g, 30.27 mmol) and concentrated aqueous HCl (37%, 6.35 mL). The suspension was stirred at reflux for 20 h. On cooling, the excess iron was filtered off and the ethanol removed under reduced pressure, causing a yellow precipitate to form. The resulting aqueous suspension was combined with $CH_2Cl_2$ (200 mL), $Na_2EDTA$ (20.2 g, 54.27 mmol), and deionized water (350 mL), and the pH of the ensemble was raised to ca. 7 (aqueous $NH_4OH$) while stirring. A concentrated $H_2O_2$ solution (30%, 1 mL) was then added and the pH further increased to ca. 8.5 (aqueous $NH_4OH$). The mixture was left stirring vigorously for 2 h before separating the organic phase and extracting the aqueous phase with 2 × 100 mL portions of $CH_2Cl_2$. The organic phases were combined, dried over $Na_2SO_4$, and evaporated to dryness to give a

(33) Desreux, J. F. iIn *Lanthanide Probes in Life, Chemical and Earth Sciences*; Bunzli, J.-C. G., Choppin, G. R., Eds.; Elsevier Publishing Co.: Amsterdam, **1989**; Chapter 2.

(34) Schwarzenbach, G. *Complexometirc Titrations*; Chapman and Hall: London, **1957**; p 8.

light brown oil. The crude product was purified by column chromatography on $Al_2O_3$ (1.5% MeOH in $CH_2Cl_2$) to give **L5** as a white solid (0.71 g, 80%). $^1$H NMR ($CDCl_3$; 500 MHz): $\delta$ 8.51 (1H, s, $H^1$), 8.39 (3H, m, $H^{12,14,23}$), 8.25 (1H, d, $J^3$ = 8.11 Hz, $H^3$), 8.01 (1H, t, $J^3 = J^3$ = 7.93 Hz, $H^{13}$), 7.93 (1H, t, $J^3 = J^3$ = 7.86 Hz, $H^{24}$), 7.73 (1H, s, $H^9$), 7.72 (1H, s, $H^{17}$), 7.70 (1H, s, $H^{20}$), 7.69 (1H, s, $H^6$), 7.64 (1H, d, $J^3$ = 8.15 Hz, $H^2$), 7.57 (1H, dd, $J^3$ = 7.65 and $J^4$ = 0.90 Hz, $H^{25}$), 7.34 (4H, m, $H^{4,11,15,22}$), 7.26 (3H, m, $H^{10,16,21}$), 7.21 (1H, dd, $J^3$ = 8.30 and $J^4$ = 1.39 Hz, $H^5$), 4.31 (2H, s, $H^{18,19}$), 4.29 (2H, s, $H^{7,8}$), 4.23 (3H, s, $Me^2$), 4.21 (3H, s, $Me^3$), 4.19 (6H, s, $Me^{4,5}$), 3.61 (2H, q, $J^3$ = 7.13 Hz, $H^{26,27}$), 3.35 (2H, $J^3$ = 7.08 Hz, $H^{28,29}$), 2.41 (3H, s, $Me^1$), 1.29 (3H, t, $J^3$ = 7.13 Hz, $Me^6$), 1.12 (3H, t, $J^3$ = 7.08, $Me^7$). Elem anal. calcd (%) for $C_{55}H_{50}N_{12}O \cdot 0.38H_2O$: C, 73.25; H, 5.67; N, 18.64. Found: C, 73.23; H, 5.63; N, 18.67. ESI-MS $m/z$: 895.8 {[**L5** + H]$^+$}, 1791.0 {[2**L5** + H]$^+$}.

**Preparation of *HHH*-[ZnLu$_2$(L5)$_3$](CF$_3$SO$_3$)$_8$.** Zn$(CF_3SO_3)_2$ (2.71 mg, $7.5 \times 10^{-3}$ mmol, 1 equiv), $Lu(CF_3SO_3)_3 \cdot 1.14H_2O$ (9.64 mg, $15.0 \times 10^{-3}$ mmol, 2 equiv) and **L5** (20.1 mg, $22.5 \times 10^{-3}$ mmol, 3 equiv) were combined in dry acetonitrile (4 mL) and stirred for 48 h at ambient temperature. Diethyl ether was then added to the pale yellow solution to precipitate the complex. The resulting solid was collected by filtration and dried in vacuo to give *HHH*-[ZnLu$_2$(**L5**)$_3$](CF$_3$SO$_3$)$_8 \cdot x$H$_2$O ($10 \leq x \leq 14$) in typical 70−90% yields. X-ray-quality prisms of *HHH*-[ZnLu$_2$(**L5**)$_3$](CF$_3$SO$_3$)$_8$ were obtained by the slow diffusion of *n*-hexane vapors into a concentrated solution of the complex in methanol. $^1$H NMR ($CD_3CN$; 500 MHz): $\delta$ 8.55 (3H, d, $J^3$ = 8.20 Hz, $H^{23}$), 8.22 (3H, t, $J^3 = J^3$ = 8.14 Hz, $H^{24}$), 8.15 (3H, d, $J^3$ = 8.44 Hz, $H^3$), 7.93 (3H, s, $H^1$), 7.76.7.86 (12 H, m, $H^{2,12,13,14}$), 7.74 (3H, d, $J^3$ = 7.96 Hz, $H^{25}$), 7.70 (3H, d, $J^3$ = 8.46 Hz, $H^{15}$), 7.57 (3H, d, $J^3$ = 8.47 Hz, $H^{11}$), 7.34 (3H, d, $J^3$ = 8.52 Hz, $H^{16}$), 7.26 (6H, m, $H^{4,22}$), 7.15 (3H, d, $J^3$ = 8.51 Hz, $H^{10}$), 6.95 (3H, d, $J^3$ = 8.49 Hz, $H^{21}$), 6.89 (3H, d, $J^3$ = 8.45 Hz, $H^5$), 5.39 (3H, s, $H^{20}$), 5.33 (3H, s, $H^9$), 5.27 (3H, s, $H^{17}$), 7.34 (3H, s, $H^6$), 4.19 (9H, s, $Me^5$), 4.06 (9H, s, $Me^2$), 4.00 (9H, s, $Me^3$), 3.92 (9H, s, $Me^4$), 3.58 (6H, m, $H^{7/8,18/19}$), 3.23−3.37 (12H, m, $H^{7/8,18/19,28,29}$), 2.70 (3H, m, $H^{26/27}$), 2.55 (3H, m, $H^{26/27}$), 2.14 (9H, s, $Me^1$), 0.92 (9H, t, $J^3$ = 7.10 Hz, $Me^7$), 0.60 (9H, t, $J^3$ = 7.08 Hz, $Me^6$). Elem anal. calcd (%) for $Lu_2ZnC_{173}H_{150}N_{36}O_{27}S_8F_{24} \cdot 11.2H_2O$: C, 46.22; H, 3.86; N, 11.21. Found: C, 46.23; H, 3.71; N, 11.14. ESI-MS $m/z$: 566.6 {[ZnLu$_2$(**L5**)$_3$(CF$_3$SO$_3$)$_2$]$^{6+}$}, 709.5 {[ZnLu$_2$(**L5**)$_3$(CF$_3$SO$_3$)$_3$]$^{5+}$}, 924.0 {[ZnLu$_2$(**L5**)$_3$(CF$_3$SO$_3$)$_4$]$^{4+}$}, 1282.1 {[ZnLu$_2$(**L5**)$_3$(CF$_3$SO$_3$)$_5$]$^{3+}$}, 1997.1 {[ZnLu$_2$(**L5**)$_3$(CF$_3$SO$_3$)$_6$]$^{2+}$}.

**Single-Crystal Structure Determination.** A summary of the crystal data, intensity measurements, and structure refinement parameters for *HHH*-[ZnLu$_2$(**L5**)$_3$](CF$_3$SO$_3$)$_8$ is collected in Table S8 (Supporting Information). Diffraction measurements were done at the Swiss-Norwegian Beamlines (SNBL) at the European Synchrotron Radiation Facility. Diffraction data were recorded at 100 K using as MAR345 Image Plate detector with a radiation of wavelength 0.72242 Å and a crystal-to-detector distance of 200 mm. A total of 445 frames with exposure times of 10 s and rotation steps of 0.5° were collected. All diffraction intensities were indexed in a triclinic lattice. A total of 42 023 diffraction intensities were integrated and corrected for Lorentz and polarization effects using CrysAlis software.[35] Solutions were generated by conventional direct methods and refined by full-matrix nonlinear least squares on all $F^2$ data using the SHELXS-97 and SHELXL software, respectively (as implemented in the SHELXTL suite of programs).[36] Empirical absorption corrections were applied on the basis of multiple and symmetry-equivalent measurements using SADABS.[37] Large channels of ca. 12 Å in diameter propagate along the [001] direction in the crystal structure of *HHH*-[ZnLu$_2$(**L5**)$_3$](CF$_3$SO$_3$)$_8$ and provide such an effective means of escape for the cocrystallized solvent that manipulation of the crystals without causing damage is virtually impossible. The inherent disorder caused by partial collapse of the crystal on removal from the mother liquor is thus reflected in the intensity data, which tended to zero at only 40° in $2\theta$. An unambiguous solution was readily obtained using standard heavy atom Patterson or direct methods procedures, but satisfactory refinement was only achievable with the extensive use of restraints and constraints. The refinement strategy adopted is as follows: (i) Similarity restraints (SAME) were applied to all 1−2 and 1−3 distances in the amide residues and aromatic rings of the ligand strands (reference geometries were either taken from the residues/rings with the most sensible and robust nonrestrained geometry or from model fragments found in the structural database). (ii) Of the eight expected triflate counterions, only five were located in interstitial positions in the electron density map (one of which occupies ca. two positions). All five were refined with rigid body constraints, with the geometries being referenced to an ordered $CF_3SO_3$ fragment found in the structural database. (iii) For 18 poorly resolved atoms, the isotropic displacement parameters exceeded 0.45 Å$^2$ on free refinement. Constraints were thus applied to prevent the displacement parameters from exceeding this value. (iv) Several groups of atoms constituting aromatic rings were restrained to be coplanar (FLAT). (v) Scattering contributions from diffuse interstitial solvent were removed using the SQUEEZE routine in PLATON.[38] Given the limitations associated with the crystal structure of *HHH*-[ZnLu$_2$(**L5**)$_3$](CF$_3$SO$_3$)$_8$, we stress that it merits no detailed analysis beyond establishing the connectivity of the complex cation. CCDC-707919 contains the supplementary crystallographic data for *HHH*-[ZnLu$_2$(**L5**)$_3$](CF$_3$SO$_3$)$_8$. The CIF file can be obtained free of charge via www.ccdc.cam.ac.uk/conts/retrieving.html (or from the Cambridge Crystallographic Data Centre, 12 Union Road, Cambridge CB2 1EZ, UK. Fax: (+ 44) 1223−336−033. E-mail: deposit@ccdc.cam.ac.uk).

**Spectroscopic and Analytical Measurements.** Electronic spectra in the UV−vis were recorded at 25 °C from solutions in $CH_3CN$ with a Perkin-Elmer Lambda 900 spectrometer using quartz cells of 0.1 or 1 mm path length. Automated spectrophotometric titrations were performed with a J & M diode array spectrometer (Tidas series) connected to an external computer. In a typical experiment, 50 mL of the ligand ($2 \times 10^{-4}$ M) in $CH_3CN$ and 0.01 M [$Bu_4N$]($CF_3SO_3$) was titrated at 25 °C with a solution of $Zn(CF_3SO_3)_2$ or $Ln(CF_3SO_3)_3 \cdot xH_2O$ ($2 \times 10^{-3}$ M) in the same solvent under an inert atmosphere. After each addition of 0.1 mL, the absorbance was recorded using Hellma optrodes (optical path length 0.1 cm) immersed in the thermostatted titration vessel and connected to the spectrometer. Batch spectrophotometric titrations were performed by preparing 40−50 solutions in MeCN (+ ca. 3% $CH_2Cl_2$) with metal/ligand ratios in the range 0.1−4.0 and ligand concentrations in the range $1 \times 10^{-4} \leq |\mathbf{L5}|_{tot} \leq 2 \times 10^{-4}$ M. The solutions were left to equilibrate for 48 h at 25 °C before recording UV−vis spectra with a Perkin-Elmer Lambda 900 spectrometer. Mathematical treatment of the spectrophotometric data was performed with factor analysis and with the SPECFIT program.[27] $^1$H and $^{13}$C NMR spectra were recorded at 25 °C on a Bruker Avance 400 or 500 MHz spectrometer. Chemical shifts are given in parts per million with respect to $CHD_2CN$. Diffusion experiments were carried out at 400 MHz Larmor frequency. Solutions ($CD_3CN$, 293 K, $|complex|_{tot} = 5 \times 10^{-3}$ M) of the complex were prepared in situ and left to equilibrate for 48 h.

(35) *CrysAlis Software Package*, Oxford Diffraction: Oxfordshire, U.K., **2006**.

(36) *SHELXTL Program System*, version 5.1; Bruker Analytical X-ray Instruments Inc.: Madison, WI, **1998**.

(37) Sheldrick, G. M. *SADABS*; University of Göttingen: Göttingen, Germany, **1996**.

(38) (a) Spek, A. L. *Acta Crystallogr.* **1990**, *A46*, C-34. (b) Spek, A. L., *PLATON*; University of Utrecht: Utrecht, The Netherlands, **2003**.

The pulse sequence used was the Bruker pulse program *ledbpgp2s*,[39] which employs a stimulated echo, bipolar gradients, and a longitudinal eddy current delay as the *z* filter. The four 2 ms gradient pulses have sine-bell shapes and amplitudes ranging linearly from 2.5 to 50 G $cm^{-1}$ in 32 steps. The diffusion delay was in the range 60−140 ms, depending on the analyte diffusion coefficient, and the number of scans was 32. The processing was done using a line broadening of 5 Hz, and the diffusion coefficients were calculated with the Bruker processing package. Pneumatically assisted electrospray (ESI-MS) mass spectra were recorded from $10^{-4}$ M solutions on a Finnigan SSQ7000 instrument. Elemental analyses were performed by Dr. H. Eder from the microchemical Laboratory of the University of Geneva. Linear least-squares fits were performed with Excel.

**Acknowledgment.** We thank P. Perrottet for carefully recording ESI-MS spectra and SNBL for in-house beam-time allocation. Financial support from the Swiss National Science Foundation, from the European Commission "Directorate D − The human factor, mobility, and Marie-Curie activities" framework, and from the Swiss Office for Science and Education within the frame of the ESF COST Action D31 are gratefully acknowledged.

(39) Wu, D; Chen, A.; Johnson, C. S.Jr. *J. Magn. Reson. A* **1995**, *115*, 260–264.

**Supporting Information Available:** Geometric parameters from the crystal structure of *HHH*-$[ZnLu_2(\mathbf{L5})_3](CF_3SO_3)_8$ (Tables S1−S4 and Schemes S1−S4). Peaks and molecular ion assignments from ESI-MS titrations (Tables S5−S7). Selected refinement parameters for the crystal structure of *HHH*-$[ZnLu_2(\mathbf{L5})_3](CF_3SO_3)_8$ (Table S8). Calculated absorption spectra for complexes of **L5** with Zn(II) and Lu(III) (Figure S1). Species distribution curves for **L5** with Zn(II) (Figure S2). Spectrophotometric titration of **L6** with Zn(II) (Figure S3). $^1$H NMR titration of **L5** with Zn(II) (Figure S4). Species distribution curves for **L5** with Lu(III) (Figure S5). Time-dependent $^1$H NMR spectra showing isomerization of a statistical 3:1 mixture of *HHT*-/*HHH*-$[Lu_2(\mathbf{L5})_3]^{6+}$ (Figure S6). Plot of $\ln|HHT|_t$ versus time (Figure S7). This material is available free of charge via the Internet at http://pubs.acs.org.